Master's thesis

NTNU
Norwegian University of Science and Technology
Faculty of Natural Sciences
Department of Physics

Eirik Jaccheri Høydalsvik

Circular dichroism in cavities coupled to ferromagnetic metals and superconductors

Master's thesis in Applied Physics and Mathematics
Supervisor: Sol H. Jacobsen
Co-supervisor: Henning Goa Hugdal
June 2023

NTNU
Norwegian University of
Science and Technology

Eirik Jaccheri Høydalsvik

Circular dichroism in cavities coupled to ferromagnetic metals and superconductors

Master's thesis in Applied Physics and Mathematics
Supervisor: Sol H. Jacobsen
Co-supervisor: Henning Goa Hugdal
June 2023

Norwegian University of Science and Technology
Faculty of Natural Sciences
Department of Physics

NTNU
Norwegian University of
Science and Technology

Abstract

In this Master thesis, we investigate the possibility of using circularly polarized light in electromagnetic cavities to study superconductors and ferromagnetic metals. An electromagnetic cavity is an enclosed space with conductive walls. When placing a material in a cavity, the interaction between the material and the cavity photons can change the effective photon spectrum. This renormalized spectrum can be measured using transmission and reflection experiments. Recently, electromagnetic cavities that can reliably excite circularly polarized photons have been developed. These cavities open up the possibility of performing polarization-dependent transmission experiments. Right- and left-handed photons transform into each other under time reversal, making circularly polarized light an important tool to study time-reversal symmetry-breaking systems. This Master thesis will examine the extent to which polarization-dependent transmission experiments can be used to probe ferromagnetic metals, ferromagnetic superconductors and time-reversal symmetry-breaking superconductors.

Sammendrag

I denne masteroppgaven undersøker vi muligheten for å bruke sirkulært polarisert lys i elektromagnetiske kaviteter for å studere superledere og ferromagnetiske metaller. En elektromagnetisk kavitet er et lukket område med elektrisk ledende vegger. Når et materiale plasseres i en kavitet, vil interaksjonen mellom materialet og kavitetfotonene endre det effektive fotonspekteret. Det effektive fotonspekteret kan måles ved hjelp av transmisjons- og refleksjonseksperimenter. Det har nylig blitt utviklet elektromagnetiske kaviteter som pålitelig kan eksitere sirkulært polariserte fotoner. Disse kavitetene muliggjør polarisasjonsavhengige transmisjonseksperimenter. Høyre- og venstrehendte fotoner transformeres til hverandre under tidsreversering. Dermed er sirkulært polarisert lys et viktig verktøy for å studere systemer som bryter tidsinversjonsymmetri. I denne masteroppgaven undesøker vi muligheten for å bruke polarisasjonsavhengige transmisjonseksperimenter til å studere ferromagnetiske metaller, ferromagnetiske superledere og superledere som bryter tidsinversjonsymmetri.

Preface

This thesis is the final work in the course "TFY4900 - Physics, Master's Thesis" and concludes the study program "Applied Physics and Mathematics" at the Norwegian University of Science and Technology. The thesis was written under the supervision of Sol H. Jacobsen and Henning Goa Hugdal.

This thesis builds on my project thesis from the course "TFY4510 - Physics, Specialization Project". The sections 2.1, 4.1 and 4.2, as well as the introduction of chapter 4, are based on similar sections from this project thesis [1].

First, I would like to thank my supervisors Sol and Henning for introducing me to the fascinating topics of superconductors and electromagnetic cavities. I thank Hennig for being generous with his time, and for sharing his extensive knowledge with me in our weekly meetings. I thank Sol for choosing an interesting research topic, and for asking insightful questions which kept me and Henning on the right track.

I want to thank my brother Roberto, father Geir, mother Letizia and partner Johanna for always suporting me. I would also like to thank my friends in Trondheim for making my time at NTNU fun and interesting.

Trondheim, Norway
June 2023

Eirik Jaccheri Høydalsvik

Contents

Chapter 1

Introduction

A circularly polarized light wave has an electromagnetic field with a constant amplitude that is rotating at a constant rate ω, and can either be right or left-handed [2]. Taking the propagation direction of the light wave to be the z-direction, a right-handed light wave rotates counterclockwise while a left-handed light wave rotates clockwise. The magnetic field of a right- and a left-handed light wave is illustrated in fig. 1.1. Time-reversal is a symmetry operation that reverses the direction of time $t \to -t$ and momentum $\mathbf{q} \to -\mathbf{q}$. Under time-reversal, right- and left-handed light waves transform into each other [3]. This property makes experiments involving circularly polarized light an important method to study time-reversal symmetry-breaking systems. One such technique is polarization-dependent absorption experiments, which measure the difference in absorption of left and right-handed light waves [4, 5]. A material that has a different absorption of left and right-handed light is said to display circular dichroism.

An electromagnetic cavity is an enclosed space with reflective material on the boundary. The reflective boundaries cause the electromagnetic field inside the cavity to form standing waves. Materials placed inside the cavity have a coupling with the standing waves which is inversely proportional to the volume of the cavity [6]. This property allows for much stronger light-matter coupling than in free space. Electromagnetic cavities where circularly polarized light can be excited reliably have been developed recently [7–9]. In this thesis, we investigate the possibility of using these cavities to probe time-reversal symmetry-breaking superconductors and ferromagnetic metals.

1.1 Superconductivity

Superconductivity is a phenomenon where a material displays zero resistivity and perfect diamagnetism under a certain critical temperature T_c [10]. In BCS theory, named after Bardeen, Cooper and Schrieffer who developed it, superconductivity is caused by a phonon-mediated attractive interaction between electrons close to the Fermi surface. Under the critical temperature T_c, this interaction causes pairs of electrons to condense into a collective state described by $\Delta^{\mathbf{Q}}_{\sigma\sigma'}(\mathbf{k})$.

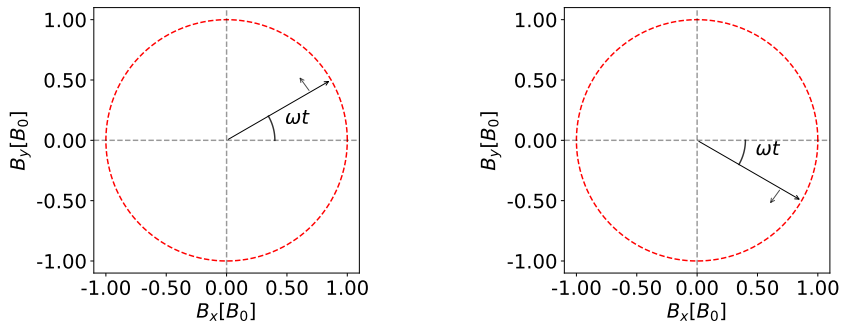

(a) Right-handed

(b) Left-handed

Figure 1.1: Arrow illustrates the magnetic field at $z = 0$ and time t for a right(a)- and left(b)-handed light wave propagating in the z-direction, with frequency ω.

The spin indices σ and σ' denote the spin direction of the electrons that make up the Cooper pair, while $\mathbf{Q}$ and $\mathbf{k}$ give the center of mass and relative momentum, respectively. In mean-field theory, the condensation is approximated as constant across the superconductor by setting $\mathbf{Q} = 0$. Using this approximation, the superconductor is described as quasiparticles with an energy gap $\Delta_{\sigma\sigma'}(\mathbf{k})$. The gap parameter $\Delta_{\sigma\sigma'}(\mathbf{k})$ is an important quantity in the study of superconductors, as it gives information about the microscopic mechanism of the superconductor.

The first known superconductors had s-wave gap parameters $\Delta_{\uparrow\downarrow}$. In a s-wave superconductor, the Cooper pairs are formed from electrons with opposite spin and the gap parameter is constant around the Fermi surface. In s-wave superconductors, the superconductivity is stable under impurity scattering, which means that it is easier to access experimentally in real samples [11]. Interest in non s-wave superconductivity increased with the discovery that the high-temperature cuprate superconductors had a d-wave pairing. d-wave superconductors are also formed with opposite spin electrons, but the gap parameter varies around the Fermi surface. The dependence of the relative momentum $\mathbf{k}$ for s-, p- and d-wave pairing is shown in fig. 1.2.

In contrast to s- and d-wave superconductors, p-wave superconductors are triplet superconductors. Triplet superconductors are even under the interchange of spins, and can either be composed of two electrons with the same spin or a symmetric superposition of electrons with opposite spin [12]. Several superconductors have been theorized to be p-wave superconductors that break time-reversal symmetry [11–15]. One such class of superconductors are the ferromagnetic superconductors. Ferromagnetic superconductors are materials where superconductivity and ferromagnetism coexist. The time-reversal symmetry is then broken below the Curie temperature, where the ferromagnetic phase transition occurs. Ferromagnetic order tends to align the electron spins, favoring triplet pairing [15]. Ferromagnetism and superconductivity have been shown to coexist experimentally in the uranium-based compounds UGe2, URhGe, and UCoGe [16–18].

Chiral superconductors are another class of superconductors that break time-

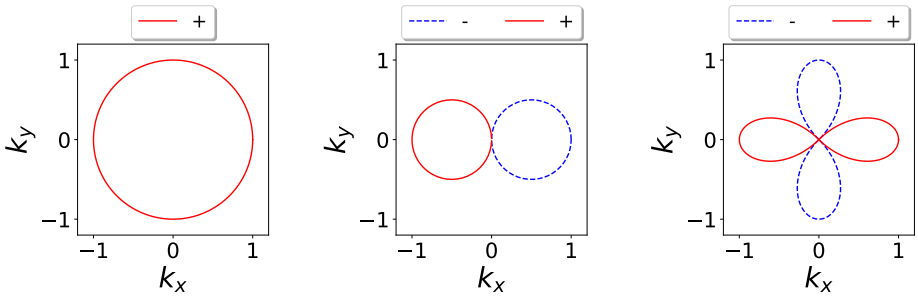

(a) s-wave (b) p-wave (c) d-wave

Figure 1.2: Polar plot of gap symetries plotted for (a) s-, (b) p- and (c) d-wave gap symmetry. The absolute value of the amplitude is given by the distance from the origin. Positive gaps are plotted in red while negative gaps are plotted in blue with a dashed line.

reversal symmetry [3, 12]. Chiral superconductivity is a topological state, where the time-reversal symmetry is spontaneously broken at the critical temperature of the superconductor. The chiral states studied in this Master thesis have the gap parameter $\Delta_{\mathbf{k}} \propto k_x \pm ik_y \propto e^{\pm i\phi}$. When moving on a closed path around the k_z-axis, $\phi \in [0, 2\pi]$, the phase of the gap parameter precesses by $\pm 2\pi$ [19]. The two states $e^{\pm i\phi}$ have opposite directions of precession, defining the chirality of the state. Under time reversal, the two gap parameters transform into each other. The time-reversal symmetry is therefore broken by the orbital part of the gap parameter, in contrast to ferromagnetic superconductors, where the time-reversal symmetry is broken by the spin degrees of freedom.

1.2 Electromagnetic cavities

An electromagnetic cavity is an enclosed space with reflective material on the boundary. The electromagnetic field inside of the cavity has standing wave solutions called mode functions. In the quantum regime, the amplitudes of the mode functions are quantized into photons [20]. In recent years, there has been great interest in studying the coupling between these photon modes and condensed matter systems [6, 21–27]. Coupling condensed matter systems and cavities can have applications in quantum information [28, 29]. This is because quantum information can be stored in a condensed matter system, and the cavity can be used to transmit the information over much greater distances than a proximity-coupled system [26, 27, 29]. One of the key advantages of studying light-matter coupling inside a cavity is that the coupling of the cavity to the material becomes inversely proportional to the cavity volume. Decreasing the cavity size can increase the light-matter coupling by several orders of magnitude, compared to its free space value [6]. Using this property, strong coupling between electromagnetic cavities and ferromagnets [23] and ferrimagnets [22], has been achieved experimentally. The strong coupling manifests itself as an anticrossing

in the photon dispersion, at the resonance frequency of the magnetic system.

Another advantage of electromagnetic cavities is the possibility of performing transmission and reflection experiments. Irradiating the cavity with a pulse of light, and recording the transmitted and reflected light gives information about the spectrum of the photons inside the cavity. If the photon modes interact with a condensed matter system, the photon dispersion gets modified, for example by forming anticrossings in the spectrum. In this way, transmission experiments can be used to study condensed matter systems. Unlike absorption experiments, transmission experiments do not rely on driving the system with periodic light waves. Therefore, transmission experiments allow you to study a system without disturbing it. For this reason, cavities are routinely used to study chemical reactions [7].

Previously, transmission and reflection experiments have been performed by exciting linearly polarized light [22, 23]. One of the inspirations for this Master project is the development of electromagnetic cavities where circularly polarized light can be excited reliably [7–9]. Such an electromagnetic cavity was already developed in 1974 to perform spin-sensitive electron paramagnetic resonance experiments [8]. In electron paramagnetic resonance experiments, a material is placed inside an electromagnetic cavity. A strong constant magnetic field is applied to the material, and the transition between the spin-up and spin-down state of the electron is excited using the cavity field. More recently, a cross resonator has been developed. A cross resonator [7–9] is composed of two rectangular microcavities which are placed orthogonal to each other to form a cross. By exciting the two microcavities 90-degrees out of phase, the light in the overlapping region becomes approximately circularly polarized [7, 9]. The cross resonator gives more precise control over the photon polarization. In addition, the microcavities allow for smaller cavity sizes which can increase photon-matter coupling and be included in miniaturized circuitry.

1.3 Circular dichroism

A material exhibits circular dichroism if the absorption of light is polarization dependent. In an absorption experiment, a material is driven by an external light wave. The transmitted intensity of the light wave is recorded, which gives the proportion of the intensity that is absorbed by the material. Measuring the differential absorption of left and right-handed light is a popular experimental technique, giving information about the spin and angular momentum of the electrons [5]. Circular dichroism in superconductors has also been studied [30–35]. Capelle et al. studied the conditions under which a conventional s-wave superconductor would give rise to dichroism [30, 31]. Yip and Sauls studied dichroism in unconventional superconductors and concluded that for the effect to exist, particle-hole symmetry must be broken in the superconductor [34]. Wysokiński et al. showed theoretically that a multiband chiral $k_x + ik_y$ superconductor would give rise to dichroism [32, 33].

In this thesis, we will modify the definition of dichroism to the cavity-material system having polarization-dependent transmission coefficients. Such a definition of dichroism has already been used in the context of chiral biomolecules [36].

The paper showed that chiral biomolecules coupled to electromagnetic cavities in the strong coupling regime, form hybrid photon-matter polariton states. The left and right-handed photons hybridize differently with the molecules, leading to a polarization-dependent transmission spectrum. The goal of this thesis is to apply the same principles to superconductors with broken time-reversal symmetry.

1.4 Structure of the thesis

The first five chapters introduce the necessary prerequisites to study circular dichroism in electromagnetic cavities. In chapters 2 and 3 we introduce topics related to electromagnetic cavities. First, we derive the expression for the quantized electromagnetic field inside a cavity. This expression is then applied to derive interaction Hamiltonians between circularly polarized photons inside the cavity and materials placed inside the cavity. The input output-formalism is also introduced to derive expressions for reflection and transmission coefficients. In chapters 4 and 5 we introduce the functional integration formalism, and the time reversal-symmetry breaking superconducting states that are studied in chapter 6. Finally, the main results are summarized and discussed in chapter 7.

Chapter 2

Electromagnetic cavities

In this thesis, we study systems that combine electromagnetic cavities and condensed matter systems, like ferromagnetic metals and superconductors. In order to study the combined system in the quantum regime, we first need a description of the quantized photon modes inside an electromagnetic cavity. We start this chapter by deriving an expression for the quantized vector potential inside a rectangular cavity with periodic boundary conditions in the xy-plane. In the following sections, we use the expression for the vector potential to derive coupling Hamiltonians between the cavity photons and condensed matter systems placed inside the cavity. These couplings are expressed in terms of circularly polarized photon modes. We conclude the chapter by discussing the time reversal of circularly polarized photon modes.

2.1 Quantization of cavity modes

We follow the derivation of Kakazu and Kim for the quantization of the electromagnetic modes inside a rectangular cavity with side lengths L_x, L_y, and L_z [20]. The walls in the z-direction are assumed to be perfectly conducting, leading to the boundary conditions $\mathbf{E}|_{tan} = \mathbf{B}|_{norm} = 0$ at $z = 0$ and $z = L_z$. $\mathbf{E}|_{tan}$ is the component of the electric field tangential to the cavity wall, and $\mathbf{B}|_{norm}$ is the component of the magnetic field that is normal to the cavity wall. Furthermore, we assume that $L_x, L_y \gg L_z$, allowing us to impose periodic boundary conditions in the x and y-directions. This cavity geometry is depicted in fig. 2.1, and the boundary conditions are satisfied by the vector potential

$$\mathbf{A} = \sum_{\mathbf{q},i} \sqrt{\frac{\hbar}{2\epsilon\epsilon_0 V w_{\mathbf{q}}}} \left(b_{\mathbf{q},i} u_{\mathbf{q},i} + b^*_{\mathbf{q},i} u^\dagger_{\mathbf{q},i} \right) , \tag{2.1}$$

with the mode functions

$$u_{\mathbf{q},x} = u_{\mathbf{q},y} = \sqrt{\frac{2}{V}} e^{iq_x x} e^{iq_y y} i \sin Q_z z,$$
$$u_{\mathbf{q},z} = \sqrt{\frac{2}{V}} e^{iq_x x} e^{iq_y y} \cos Q_z z \ . \tag{2.2}$$

When $n_z = 0$ the definition of $u_{\mathbf{q},z}$ is modified to be

$$u_{\mathbf{q},z} = \sqrt{\frac{1}{V}} e^{iq_x x} e^{iq_y y} \ . \tag{2.3}$$

Here V is the volume of the cavity, $\hbar$ is the reduced Planck constant, ϵ_0 is the vacuum permittivity, ϵ is the relative permittivity inside the cavity, c_0 is the speed of light in vacuum, $c = c_0/\sqrt{\epsilon}$ is the speed of light inside the cavity, $\omega_{\mathbf{q}} = |c\mathbf{q}|$ is the frequency of the electromagnetic wave and $b_{\mathbf{q},i}$ is the field amplitude in the $\hat{e}_i$ direction. The wave vector can take the values $\mathbf{q} = (2\pi n_x/L_x, 2\pi n_y/L_y, \pi n_z/L_z)$, with $n_x, n_y = 0, \pm 1, \pm 2...$ and $n_z = 0, 1, 2....$

Because of the gauge freedom in the vector potential $\mathbf{A}$, the field amplitudes $b_{\mathbf{q},i}$ are not independent. Choosing the Coulomb gauge, the vector potential must be transversal to its propagation direction, $\mathbf{A}_{\mathbf{q}} \cdot \mathbf{q} = 0$. To take advantage of the transversality, we rotate to a new basis $\bar{e}_{\mathbf{q},s}, s \in (1, 2, 3)$, where the new z-axis (labeled by 3) is parallel to $\mathbf{q}$. The new basis vectors are given by $\bar{e}_{\mathbf{q},s} = \sum_i O^{\mathbf{q}}_{si} \hat{e}_i$, with

$$O^{\mathbf{q}} = \begin{pmatrix} \cos\theta\cos\phi & \cos\theta\sin\phi & -\sin\theta \\ -\sin\phi & \cos\phi & 0 \\ \sin\phi\cos\phi & \sin\theta\sin\phi & \cos\theta \end{pmatrix} \ , \tag{2.4}$$

where the angles θ and ϕ depend on $\mathbf{q}$. The field amplitudes in this basis become $a_{\mathbf{q},s} = \sum_i O^{\mathbf{q}}_{s,i} b_{\mathbf{q},i}$ and $a^*_{\mathbf{q},s} = \sum_i O^{\mathbf{q}}_{s,i} b^*_{\mathbf{q},i}$. Written in this basis, the vector potential becomes

$$\mathbf{A} = \sum_{\mathbf{q},s} \sqrt{\frac{\hbar}{2\epsilon\epsilon_0 V \omega_{\mathbf{q}}}} \left(a_{\mathbf{q},s} \bar{u}_{\mathbf{q},s} + a^*_{\mathbf{q},s} \bar{u}^\dagger_{\mathbf{q},s} \right) \ , \tag{2.5}$$

where we have defined the new mode functions $\bar{u}_{\mathbf{q},s} = \sum_i \bar{e}_{q,i} O^{\mathbf{q}}_{s,i} u_{\mathbf{q},i}$. Using the facts that the field amplitudes are now independent and that the mode functions are orthogonal $\int_c \bar{u}_{\mathbf{q},s} \cdot \bar{u}_{\mathbf{q}',s'} = \delta_{s,s'} \delta_{\mathbf{q},\mathbf{q}'}$, the field amplitudes can be quantized using the canonical quantization procedure [10]

$$\mathbf{A} = \sum_{\mathbf{q},s} \sqrt{\frac{\hbar}{2\epsilon\epsilon_0 V \omega_{\mathbf{q}}}} \left(a_{\mathbf{q},s} \bar{u}_{\mathbf{q},s} + a^\dagger_{\mathbf{q},s} \bar{u}^\dagger_{\mathbf{q},s} \right) \ . \tag{2.6}$$

In the last line, $a^\dagger$ and a are operators with the bosonic commutation relations

$$\begin{aligned} [a_{\mathbf{q},s}, a_{\mathbf{q}',s'}] &= \left[a^\dagger_{\mathbf{q},s}, a^\dagger_{\mathbf{q}',s'} \right] = 0, \\ \left[a_{\mathbf{q},s}, a^\dagger_{\mathbf{q}',s'} \right] &= i\hbar \delta_{\mathbf{q},\mathbf{q}'} \delta_{s,s'} \ . \end{aligned} \tag{2.7}$$

Using the expression for the quantized vector potential given in eq. (2.6), we can proceed to derive the quantized Hamiltonian for the electromagnetic cavity, including interactions between the cavity photons and condensed matter systems.

When deriving these interactions, we will make the approximation that $n_z = 1$ in eq. (2.6). Each increment of n_z has an associated energy cost of $\hbar c\pi/L_z$. Since $L_z \ll L_x, L_y$, high n_z excitations are energetically costly. However, the $n_z = 0$ modes have zero in-plane electric field which would make the paramagnetic coupling discussed in section 2.5 vanish. As for the Zeeman coupling discussed in section 2.4, the $n_z = 0$ mode only couples to one of the linear polarization's s [37] and can therefore not give rise to circular dichroism. The in-plane electric and magnetic field for the $n_z = 1$ modes are illustrated in figs. 2.1 and 2.2. We now change the definition of $\mathbf{q}$ to be the in-plane momentum $\mathbf{q} = (2\pi n_x/L_x, 2\pi n_y/L_y)$, the z-component $Q_z = \pi/L_z$ and the frequency

$$\omega_{\mathbf{q}} = c\sqrt{\mathbf{q}^2 + Q_z^2} \, . \tag{2.8}$$

2.2 Quantized Hamiltonian

Classically the Hamiltonian for an electromagnetic field without interactions is given by [38]

$$H_0 = \frac{\epsilon_0}{2} \int d\mathbf{r} \left[\left(\partial_t \mathbf{A}(r,t)\right)^2 + \frac{1}{\mu_0} \left(\nabla \times \mathbf{A}(r,t)\right)^2 \right] \, . \tag{2.9}$$

Inserting the expression for the quantized vector potential eq. (2.6) and using the identity $\int_c \bar{u}_{\mathbf{q},s} \cdot \bar{u}_{\mathbf{q}',s'} = \delta_{s,s'}\delta_{\mathbf{q},\mathbf{q}'}$, gives the quantized Hamiltonian

$$H_0 = \sum_{\mathbf{q},s} \hbar\omega_{\mathbf{q}} a^\dagger_{\mathbf{q},s} a_{\mathbf{q},s} \, , \tag{2.10}$$

where $s \in \{1, 2\}$ gives the linear polarization of the photon mode. As expected, the Hamiltonian is composed of independent harmonic oscillators for each momentum $\mathbf{q}$ and linear polarization s.

In order to study circular dichroism, it is necessary to change to a basis of circularly polarized light. A circularly polarized photon is a linear combination of two linearly polarized photons, with a $\pm\pi/2$ phase difference between the polarizations. Written as a matrix equation, the relation between circularly and linearly polarized light is given by

$$\begin{bmatrix} a_{\mathbf{q},\mathrm{L}} \\ a_{\mathbf{q},\mathrm{R}} \end{bmatrix} = \frac{1}{\sqrt{2}} \begin{bmatrix} 1 & -i \\ 1 & i \end{bmatrix} \begin{bmatrix} a_{\mathbf{q},1} \\ a_{\mathbf{q},2} \end{bmatrix} \, , \tag{2.11}$$

Where $a_{\mathbf{q},\mathrm{L}}$ is the annihilation operator for a left-handed photon and $a_{\mathbf{q},\mathrm{R}}$ is the annihilation operator for a right-handed photon. Using the fact that this transformation is unitary, we can perform a basis change in eq. (2.10)

$$H_0 = \sum_{\mathbf{q},l} \hbar\omega_{\mathbf{q}} a^\dagger_{\mathbf{q},l} a_{\mathbf{q},l} \, , \tag{2.12}$$

where $l \in \{\mathrm{R}, \mathrm{L}\}$. In this thesis, we want to consider an electromagnetic cavity interacting with an electronic system. The Hamiltonian for an electronic system interacting with the electromagnetic cavity is given by

$$H = \sum_{\mathbf{q},l} \hbar\omega_{\mathbf{q}} a^\dagger_{\mathbf{q},l} a_{\mathbf{q},l} + \sum_{\mathbf{k}\sigma\sigma'} \epsilon_{\mathbf{k}\sigma\sigma'} C^\dagger_{\mathbf{k}\sigma} C_{\mathbf{k}\sigma'} + H_{\mathrm{int}}(C^\dagger, C, a^\dagger, a) \, . \tag{2.13}$$

In the last line $C^\dagger$ and C are electron creation/annihilation-operators, the second term gives the non-interacting electron theory, and H_{int} is the Hamiltonian describing the interaction between the photons and the electrons. For a free electron gas, $\epsilon_{\mathbf{k}\sigma\sigma'} = \frac{\hbar^2|\mathbf{k}|^2}{2m_e}\delta_{\sigma\sigma'} - \mu$, where μ is the chemical potential. When the electronic system is a superconductor, additional $C^\dagger C^\dagger$ and CC terms must be added to eq. (2.13). The non-interacting superconductor theories will be considered in chapter 5.

The following sections are devoted to the interaction Hamiltonian H_{int}. First, we show how to convert H_{int} to a basis of circularly polarized light. In the following sections, we present the specific coupling terms that we will consider in this thesis.

2.3 Circularly polarized basis

In this thesis, we consider the paramagnetic and Zeeman coupling. The Hamiltonian for both these couplings can be written in the form

$$H_{int} = \sum_{\mathbf{k}\mathbf{k}'\sigma\sigma' s} g^{\mathbf{k}\mathbf{k}'}_{\sigma\sigma' s} C^\dagger_{\mathbf{k},\sigma} C_{\mathbf{k}',\sigma'} \left(a_{\mathbf{k}-\mathbf{k}',s} + a^\dagger_{\mathbf{k}'-\mathbf{k},s} \right) \, , \tag{2.14}$$

where s gives the linear polarization of the photon mode, σ gives the electron spin and $g^{\mathbf{k}\mathbf{k}'}_{\sigma\sigma' s}$ is the coupling parameter. In order to investigate circular dichroism, we convert eq. (2.14) to a basis of circularly polarized light using eq. (2.11)

$$\begin{aligned} H_{int} = \sum_{\mathbf{k}\mathbf{k}'\sigma\sigma'} \Big[& \frac{g^{\mathbf{k}\mathbf{k}'}_{\sigma\sigma' 1}}{\sqrt{2}} \left(a_{\mathbf{k}'-\mathbf{k}\mathrm{L}} + a_{\mathbf{k}'-\mathbf{k}\mathrm{R}} + a^\dagger_{\mathbf{k}-\mathbf{k}'\mathrm{L}} + a^\dagger_{\mathbf{k}-\mathbf{k}'\mathrm{R}} \right) \\ & + i \frac{g^{\mathbf{k}\mathbf{k}'}_{\sigma\sigma' 2}}{\sqrt{2}} \left(a_{\mathbf{k}'-\mathbf{k}\mathrm{L}} - a_{\mathbf{k}'-\mathbf{k}\mathrm{R}} - a^\dagger_{\mathbf{k}-\mathbf{k}'\mathrm{L}} + a^\dagger_{\mathbf{k}-\mathbf{k}'\mathrm{R}} \right) \Big] C^\dagger_{\mathbf{k}\sigma} C_{\mathbf{k}'\sigma'} \\ = \sum_{\mathbf{k}\mathbf{k}'\sigma\sigma'} \Big[& \frac{1}{\sqrt{2}} \left(g^{\mathbf{k}\mathbf{k}'}_{\sigma\sigma' 1} + i g^{\mathbf{k}\mathbf{k}'}_{\sigma\sigma' 2} \right) \left(a_{\mathbf{k}'-\mathbf{k}\mathrm{L}} + a^\dagger_{\mathbf{k}-\mathbf{k}'\mathrm{R}} \right) \\ & + \frac{1}{\sqrt{2}} \left(g^{\mathbf{k}\mathbf{k}'}_{\sigma\sigma' 1} - i g^{\mathbf{k}\mathbf{k}'}_{\sigma\sigma' 2} \right) \left(a_{\mathbf{k}'-\mathbf{k}\mathrm{R}} + a^\dagger_{\mathbf{k}-\mathbf{k}'\mathrm{L}} \right) \Big] C^\dagger_{\mathbf{k}\sigma} C_{\mathbf{k}'\sigma'} \, . \end{aligned} \tag{2.15}$$

or written more compactly

$$H_{int} = \sum_{\mathbf{k}\mathbf{k}'\sigma\sigma' l} g^{\mathbf{k}\mathbf{k}'}_{\sigma\sigma' l} \left(a_{\mathbf{k}'-\mathbf{k}l} + a^\dagger_{\mathbf{k}-\mathbf{k}'-l} \right) C^\dagger_{\mathbf{k}\sigma} C_{\mathbf{k}'\sigma'} \, , \tag{2.16}$$

where $l \in \{\mathrm{L}, \mathrm{R}\}$, we take $-l$ to be the opposite handedness of l and

$$g^{\mathbf{k}\mathbf{k}'}_{\sigma\sigma'\mathrm{L/R}} = \frac{1}{\sqrt{2}} \left(g^{\mathbf{k}\mathbf{k}'}_{\sigma\sigma' 1} \pm i g^{\mathbf{k}\mathbf{k}'}_{\sigma\sigma' 2} \right) \, . \tag{2.17}$$

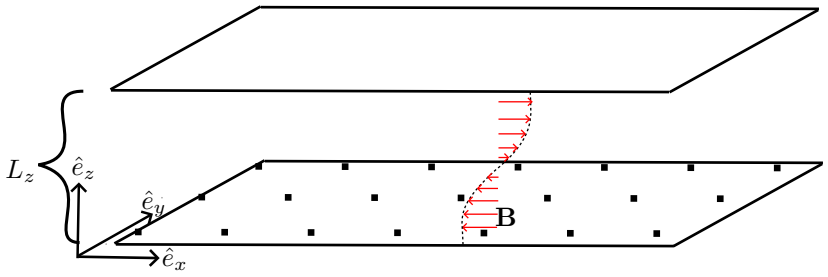

Figure 2.1: Electromagnetic cavity composed of two large sheets of reflecting material placed at $z = 0$ and $z = L_z$. Condensed matter system placed at $z \approx 0$. In-plane magnetic field $\mathbf{B}$ for $n_z = 1$ mode illustrated, showing maxima at the top and bottom of the cavity $z = 0$ and $z = L_z$.

2.4 Zeeman coupling

The Zeeman coupling describes the interaction between the electron spin and a magnetic field. When looking for circular dichroism, the Zeeman coupling is a natural choice when the time-reversal symmetry is broken for the spin degrees of freedom. Examples of such systems are ferromagnets and non-unitary superconductors. In the center of the cavity, the magnetic field points purely in the z-direction [20]. For a magnetic field in the z-direction, it can be verified that the coupling of left- and right-handed photons only differs by a phase, which would not lead to dichroism. The coupling is therefore computed at the bottom of the cavity where the in-plane magnetic field is maximal [20]. An illustration of the setup is given in fig. 2.1. The Hamiltonian for the Zeeman interaction is given by

$$\begin{aligned} H_{\text{Zeeman}} &= \sum_i \boldsymbol{\mu} \cdot \mathbf{B}_i \\ &= \sum_{\mathbf{k}\mathbf{k}' i\sigma\sigma'} \mu_B \boldsymbol{\sigma}_{\sigma\sigma'} e^{i(\mathbf{k}-\mathbf{k}')\cdot\mathbf{r}_i} C^\dagger_{\mathbf{k}\sigma} C_{\mathbf{k}'\sigma'} \cdot \nabla \times \mathbf{A}_i \ . \end{aligned} \tag{2.18}$$

Using eq. (2.6) we can compute the cross product giving

$$\begin{aligned} \nabla \times \mathbf{A} &= (\partial_y A_z - \partial_z A_y)\,\hat{e}_x + (\partial_z A_x - \partial_x A_z)\,\hat{e}_y \\ &= \sum_{\mathbf{q},s} \sqrt{\frac{\hbar}{2\epsilon_0 \omega_{\mathbf{q}}}} \left(a_{\mathbf{q},s} + a^\dagger_{-\mathbf{q},s}\right) \\ &\quad \times \left(\left(O^{\mathbf{q}}_{s,z}\partial_y u_{\mathbf{q},z} - O^{\mathbf{q}}_{s,y}\partial_z u_{\mathbf{q},y}\right)\hat{e}_x + \left(O^{\mathbf{q}}_{s,x}\partial_z u_{\mathbf{q},x} - O^{\mathbf{q}}_{s,z}\partial_x u_{\mathbf{q},z}\right)\hat{e}_y\right) \\ &= \sum_{\mathbf{q},s} \sqrt{\frac{\hbar}{\epsilon_0 V \omega_{\mathbf{q}}}} \left(a_{\mathbf{q},s} + a^\dagger_{-\mathbf{q},s}\right) e^{i\mathbf{q}\cdot\mathbf{r}_i} \\ &\quad \times \left(\left(O^{\mathbf{q}}_{s,z} i q_y - O^{\mathbf{q}}_{s,y} i Q_z\right)\hat{e}_x + \left(O^{\mathbf{q}}_{s,x} i Q_z - O^{\mathbf{q}}_{s,z} i q_x\right)\hat{e}_y\right) \ . \end{aligned} \tag{2.19}$$

Now we can simplify the expression by noting that $Q_z >> q_x, q_y$. The dominant part of the magnetic field is therefore given by

$$\begin{aligned}\nabla \times \mathbf{A} =& iQ_z \sum_{\mathbf{q},s} \sqrt{\frac{\hbar}{\epsilon_0 V \omega_{\mathbf{q}}}} \left(a_{\mathbf{q},s} + a^{\dagger}_{-\mathbf{q},s}\right) e^{i(q_x x + q_y y)} \\ & \times \left(-O^{\mathbf{q}}_{s,y}\hat{e}_x + O^{\mathbf{q}}_{s,x}\hat{e}_y\right) \ ,\end{aligned} \tag{2.20}$$

which gives the Hamiltonian

$$\begin{aligned}H_{\text{Zeeman}} =& iQ_z \sum_{\mathbf{q},\mathbf{k},\mathbf{k'},s} \sqrt{\frac{\hbar\mu_B^2}{\epsilon_0 V \omega_{\mathbf{q}}}} \delta_{q,k'-k} \left(-O^{\mathbf{q}}_{s,y}\sigma^x_{\sigma\sigma'} + O^{\mathbf{q}}_{s,x}\sigma^y_{\sigma\sigma'}\right) \\ & \times \left(a_{\mathbf{q},s} + a^{\dagger}_{-\mathbf{q},s}\right) C^{\dagger}_{\mathbf{k}\sigma} C_{\mathbf{k'}\sigma'} \ .\end{aligned} \tag{2.21}$$

Introducing the coupling coeficient $g^{\mathbf{q}}_{\sigma\sigma' s}$, defined as

$$\begin{aligned}g^{\mathbf{q}}_{\sigma\sigma' 1} &= iQ_z \sqrt{\frac{\hbar\mu_B^2}{\epsilon_0 V \omega_{\mathbf{q}}}} \left(-O^{\mathbf{q}}_{1,y}\sigma^x_{\sigma\sigma'} + O^{\mathbf{q}}_{1,x}\sigma^y_{\sigma\sigma'}\right) \\ &= -Q_z \sqrt{\frac{\hbar\mu_B^2}{\epsilon_0 V \omega_{\mathbf{q}}}} \begin{bmatrix} 0 & -e^{-i\phi} \\ e^{i\phi} & 0 \end{bmatrix} \ ,\end{aligned} \tag{2.22}$$

similarly for $s = 2$ we get

$$\begin{aligned}g^{\mathbf{q}}_{\sigma\sigma' 2} &= iQ_z \sqrt{\frac{\hbar\mu_B^2}{\epsilon_0 V \omega_{\mathbf{q}}}} \left(-O^{\mathbf{q}}_{2,y}\sigma^x_{\sigma\sigma'} + O^{\mathbf{q}}_{2,x}\sigma^y_{\sigma\sigma'}\right) \\ &= -iQ_z \sqrt{\frac{\hbar\mu_B^2}{\epsilon_0 V \omega_{\mathbf{q}}}} \begin{bmatrix} 0 & e^{-i\phi} \\ e^{i\phi} & 0 \end{bmatrix} \ .\end{aligned} \tag{2.23}$$

Written in terms of the coupling coeficients eq. (2.22) and eq. (2.23) the Hamiltonian becomes

$$H_{\text{Zeeman}} = \sum_{\mathbf{k}\mathbf{k'}\sigma\sigma' s} g^{\mathbf{k'}-\mathbf{k}}_{\sigma\sigma' s} \left(a_{\mathbf{k'}-\mathbf{k}s} + a^{\dagger}_{\mathbf{k}-\mathbf{k'}s}\right) C^{\dagger}_{\mathbf{k}\sigma} C_{\mathbf{k'}\sigma'} \ . \tag{2.24}$$

We proceed to change eq. (2.24) to a circularly polarized basis using eq. (2.16) and eq. (2.17)

$$\begin{aligned}g^{\mathbf{q}}_{\sigma\sigma' l} &= \frac{1}{\sqrt{2}} \left(g^{\mathbf{k'}-\mathbf{k}}_{\sigma\sigma' 1} \pm i g^{\mathbf{k'}-\mathbf{k}}_{\sigma\sigma' 2}\right) \\ &= Q_z \sqrt{\frac{\hbar\mu_B^2}{2\epsilon_0 V \omega_{\mathbf{q}}}} \left(\begin{bmatrix} 0 & e^{-i\phi} \\ -e^{i\phi} & 0 \end{bmatrix} \pm \begin{bmatrix} 0 & e^{-i\phi} \\ e^{i\phi} & 0 \end{bmatrix}\right) \\ &= \tilde{g}_{\text{z}} \begin{bmatrix} 0 & e^{-i\phi}\delta_{l,\text{L}} \\ -e^{i\phi}\delta_{l,\text{R}} & 0 \end{bmatrix} \ ,\end{aligned} \tag{2.25}$$

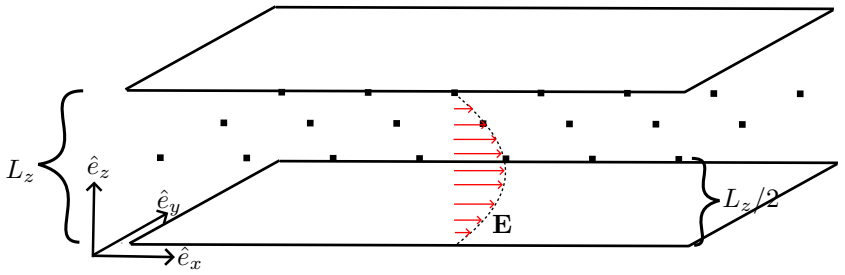

Figure 2.2: Electromagnetic cavity composed of two large sheets of reflecting material placed at $z = 0$ and $z = L_z$. Condensed matter system placed at $z = L_z/2$. In-plane electric field $\mathbf{E}$ for $n_z = 1$ mode illustrated, showing a maximum in the center of the cavity $z = L_z/2$.

where we have defined $\tilde{g}_z = Q_z\sqrt{\frac{2\hbar\mu_B^2}{\epsilon_0 V\omega_\mathbf{q}}}$. Written in this basis the action becomes

$$H_{\text{Zeeman}} = \sum_{\mathbf{k}\mathbf{k}'\sigma\sigma' l} g^{\mathbf{k}\mathbf{k}'}_{\sigma\sigma' s}\left(a_{\mathbf{k}'-\mathbf{k}l} + a^\dagger_{\mathbf{k}-\mathbf{k}'-l}\right) C^\dagger_{k\sigma}C_{k'\sigma'} \ . \tag{2.26}$$

From the coupling in eq. (2.25), one can see that right-handed photons can flip the spin of the electron from up to down, while left-handed photons can flip the spin from down to up. Since total angular momentum is conserved in the process, one can deduce that the left-handed photons have angular momentum $+\hbar$ while the right-handed photons have angular momentum $-\hbar$ [2].

2.5 Paramagnetic coupling

The paramagnetic coupling describes the interaction between the photons in the cavity and the flow of charge in a metal. The in-plane electric field is maximal in the center of the cavity [20, 27], the material is therefore placed at the center of the cavity to maximize the coupling. The setup is illustrated in fig. 2.2. The derivation of the paramagnetic coupling is left out of this thesis but can be found in [1, 6]. The Hamiltonian for the paramagnetic coupling is given by

$$H_{\text{int}} = \sum_{\mathbf{k}\mathbf{q}\sigma l} g^l_{\mathbf{k},\mathbf{k}'}\left(a_{\mathbf{k}-\mathbf{k}',l} + a^\dagger_{\mathbf{k}'-\mathbf{k},-l}\right) C^\dagger_{\mathbf{k},\sigma}C_{\mathbf{k}',\sigma} \ , \tag{2.27}$$

where $C^\dagger$ and C are the electron creation/annihilation operators and the coupling coefficient is given by

$$g^{\text{L/R}}_{\mathbf{k},\mathbf{k}'} = i\tilde{g}_\text{p}\frac{\left(O^{\mathbf{k}-\mathbf{k}'}_{1,i} \pm iO^{\mathbf{k}-\mathbf{k}'}_{2,i}\right)\frac{\mathbf{k}_i+\mathbf{k}'_i}{2}}{\left(1+\left(c\frac{\mathbf{k}-\mathbf{k}'}{\omega_0}\right)^2\right)^{1/4}} \ . \tag{2.28}$$

In the last line $O^{\mathbf{k}-\mathbf{k}'}_{s,i}$ is an element of the matrix given in eq. (2.4), we defined $\omega_0 = c\pi/L_z$, and the constant $\tilde{g}_\text{p} = \sqrt{4\alpha/(V\sqrt{\epsilon})}$, where α equals the fine

structure constant and V is the volume of the cavity. We note that $g^l_{-\mathbf{k}',-\mathbf{k}} = -g^l_{\mathbf{k},\mathbf{k}'} = g^l_{\mathbf{k}',\mathbf{k}}$.

Unlike the Zeeman coupling, the left and right-handed coupling has the same spin structure. The spin structure is not forced by conservation of angular momentum, because the photons are coupled to the orbital part of the wave function. Conservation of angular momentum is then insured by the orbital angular momentum of the electrons, and not the spin.

2.6 Time reversal symmetry

We conclude the chapter with a discussion of time-reversal symmetry. To illustrate the effect of time-reversal symmetry we calculate the magnetic field at the bottom of the cavity for a circularly polarized mode with momentum $\mathbf{q}$. By changing the basis of eq. (2.1) using eq. (2.11), we get the vector potential of a circularly polarized mode

$$\mathbf{A}_{\mathrm{R/L}}(\mathbf{r},t) = \sqrt{\frac{\hbar}{2\epsilon\epsilon_0 V\omega_{\mathbf{q}}}}\left(a_{\mathbf{q},\mathrm{R/L}}(t)\bar{u}_{\mathbf{q},\mathrm{R/L}} + a^*_{\mathbf{q},\mathrm{R/L}}(t)\bar{u}^*_{\mathbf{q},\mathrm{R/L}}\right) , \tag{2.29}$$

where the mode functions are defined as

$$\bar{u}_{\mathbf{q},\mathrm{R/L}} = \frac{\bar{u}_{\mathbf{q}1} \mp i\bar{u}_{\mathbf{q}2}}{\sqrt{2}} . \tag{2.30}$$

The field amplitudes $a_{\mathbf{q},\mathrm{R/L}}(t)$ must solve the wave equation and are therefore given by $a_{\mathbf{q},\mathrm{R/L}}(t) = a_{\mathbf{q},\mathrm{R/L}}(0)e^{-i\omega_{\mathbf{q}}t}$ [20]. We take $a_{\mathbf{q},\mathrm{R/L}}(0)$ to be real by fixing the initial phase and expanding eq. (2.29) in the linearly polarized mode functions

$$\begin{aligned}\mathbf{A}_{\mathrm{R/L}}(\mathbf{r},t) =& a_{\mathbf{q},\mathrm{R/L}}(0)\sqrt{\frac{\hbar}{4\epsilon\epsilon_0 V\omega_{\mathbf{q}}}}\Big(e^{-i\omega_{\mathbf{q}}t}\bar{u}_{\mathbf{q},1} + e^{i\omega_{\mathbf{q}}t}\bar{u}^*_{\mathbf{q},1} \\ &+ e^{\mp i\pi/2 - i\omega_{\mathbf{q}}t}\bar{u}_{\mathbf{q},2} + e^{-(\mp i\pi/2 - i\omega_{\mathbf{q}}t)}\bar{u}^*_{\mathbf{q},2}\Big) ,\end{aligned} \tag{2.31}$$

The dominant part of this magnetic field can be calculated in the same way as eq. (2.20). Performing the calculation gives

$$\mathbf{B}_{\mathrm{R/L}} = \mathbf{B}_0\left(\cos\left(\omega_{\mathbf{q}}t - \mathbf{q}\cdot\mathbf{r}\right)\tilde{e}_1 \pm \sin\left(\omega_{\mathbf{q}}t - \mathbf{q}\cdot\mathbf{r}\right)\tilde{e}_2\right) , \tag{2.32}$$

where we defined $\mathbf{B}_0 = Q_z a_{\mathbf{q}\mathrm{R/L}}\sqrt{\frac{\hbar}{2\epsilon_0 V\omega_{\mathbf{q}}}}$ and the new basis is given by $\tilde{e}_s = \left(-O^{\mathbf{q}}_{s,y}\hat{e}_x + O^{\mathbf{q}}_{s,x}\hat{e}_y\right)$. We note that the new basis is orthogonal $\tilde{e}_s \cdot \tilde{e}_{s'} = \delta_{ss'}$.

Time reversal has the effect of changing the sign of the time and the wave vector $t, \mathbf{k} \to -t, -\mathbf{k}$ [3]. Applying the time reversal operation to eq. (2.32), and using the identities $\cos(-x) = \cos x$ and $\sin(-x) = -\sin x$ gives

$$\mathbf{B}^{\mathrm{TR}}_{\mathrm{R/L}} = \mathbf{B}_0\left(\cos\left(\omega_{\mathbf{q}}t - \mathbf{q}\cdot r\right)\tilde{e}_1 \mp \sin\left(\omega_{\mathbf{q}}t - \mathbf{q}\cdot r\right)\tilde{e}_2\right) . \tag{2.33}$$

From eq. (2.33) it is clear that time reversal switches the handedness of a circularly polarized light wave. This fact has the consequence that a system must break time-reversal symmetry in order to display circular dichroism. This is because of the fact that if the system possesses time-reversal symmetry, switching left and right-handed photons would not change the Hamiltonian, and therefore left and right-handed photons must behave in exactly the same way.

Time-reversal symmetry can be broken both explicitly and spontaneously. An example of explicitly breaking time-reversal symmetry is applying an external magnetic field. Classically $\mathbf{F} = \mathbf{v} \times \mathbf{B}$, time reversal changes the sign of $\mathbf{v}$ and therefore changes the sign of the force. Examples of systems with spontaneously broken time-reversal symmetry are ferromagnets and chiral superconductors. The possibility of circular dichroism in these systems will be considered in chapter 6. It is important to note that time-reversal symmetry breaking is a necessary but not sufficient condition for dichroism. As we will see in chapter 6, many systems with broken time-reversal symmetry do not display dichroism.

Chapter 3

Input-output formalism

The input-output formalism is a useful tool from quantum optics where the cavity is coupled to an external field, and where one can calculate the output state of the external field based on the input state [39]. Crucially for this master thesis, the input-output formalism allows us to calculate transmission and reflection coefficients. These coefficients give the proportion of light that is reflected and transmitted when the cavity is irradiated with a light pulse of a given frequency. Reflection and transmission experiments are a common way to study the coupling between cavities and matter [22, 23]. In this chapter, we derive the reflection and transmission coefficients and discuss how they can be used to study dichroism. All the derivations in this chapter are based on [39].

3.1 Reflection coefficient

The simplest illustration of the input-output formalism is the calculation of the reflection coefficient for a one-sided cavity. A one-sided cavity is the same as the two-sided cavity shown in fig. 3.1 but with only one interface coupling the cavity to the environment, where the input and output field is given by $b_{\mathrm{OUT}}/b_{\mathrm{IN}}$. The cavity is modeled as a single mode a. This approximation corresponds to taking the dipole approximation $\mathbf{q} = 0$ in eq. (2.12). The cavity mode a is governed by H_{sys}, the environment is modeled as a heat bath H_{B} and the cavity and environment are coupled by H_{int}

$$\begin{aligned} H &= H_{\mathrm{sys}} + H_{\mathrm{B}} + H_{\mathrm{int}} \ , \\ H_{\mathrm{B}} &= \hbar \int d\omega b^{\dagger}(\omega) b(\omega) \ , \\ H_{\mathrm{int}} &= i\hbar \int d\omega g \left(b(\omega) a^{\dagger} - a b^{\dagger}(\omega) \right) \ , \end{aligned} \tag{3.1}$$

where $g := \sqrt{\gamma/2\pi}$ is the coupling constant between the system and the environment. The Heisenberg equation of motion for the bath reads

$$\dot{b}(t,\omega) = -i\omega b(t,\omega) + g(\omega) a(t) \ , \tag{3.2}$$

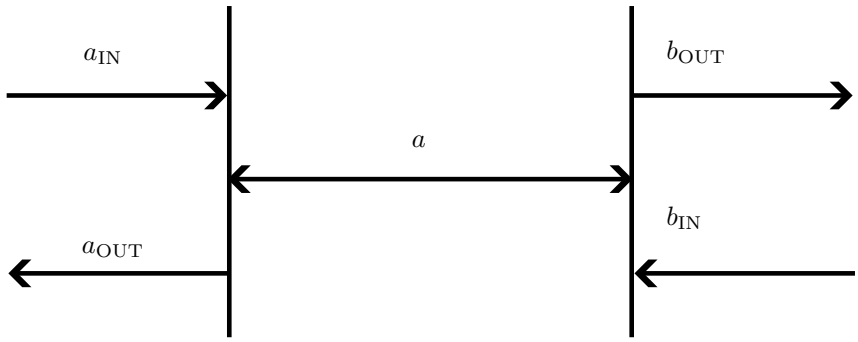

Figure 3.1: Cavity mode a coupled to two input fields $a_{\mathrm{IN/OUT}}$ and $b_{\mathrm{IN/OUT}}$

which has the solution

$$b(t,\omega) = e^{-i\omega(t-t_o)}b_0(\omega) + g\int_{t_0}^{t} e^{-i\omega(t-t')}a(t')dt' \ . \tag{3.3}$$

The equation of motion of the cavity mode reads

$$\dot{a} = -\frac{i}{\hbar}[H_{\mathrm{sys}}, a] - g\int d\omega b(t,\omega) \ , \tag{3.4}$$

inserting the solution for the bath eq. (3.3) gives

$$\dot{a} = -\frac{i}{\hbar}[H_{\mathrm{sys}}, a] - g\int_{-\infty}^{\infty} d\omega e^{-i\omega(t-t_0)}b_0(\omega) \tag{3.5}$$

$$+ g^2\int_{-\infty}^{\infty} d\omega \int_{t_0}^{t} e^{-i\omega(t-t')}a(t')dt' \ . \tag{3.6}$$

We now define the input field as the state of the environment at $t = t_0$

$$a_{\mathrm{IN}}(t) = -g\int_{-\infty}^{\infty} d\omega e^{-i\omega(t-t_0)}b_0(\omega) \ . \tag{3.7}$$

Using this definition, changing the order of integration and using Dirac delta function identities gives the equation

$$\dot{a} = -\frac{i}{\hbar}[H_{\mathrm{sys}}, a] + \frac{\gamma}{2}a(t) + \sqrt{\gamma}a_{\mathrm{IN}}(t) \ . \tag{3.8}$$

One can in a similar way derive an equation for the outgoing field. Using these two equations one can derive

$$a_{\mathrm{IN}}(t) + a_{\mathrm{OUT}}(t) = \sqrt{\gamma}a(t) \ . \tag{3.9}$$

Taking $H_{\text{sys}} = \hbar\omega_0 a^\dagger a$ in eq. (3.8), gives the equation

$$\dot{a} = -i\omega_0 a + \frac{\gamma}{2}a(t) + \sqrt{\gamma}a_{\text{IN}}(t) \ . \tag{3.10}$$

Going to Fourier space gives

$$\left[i\left(\omega - \omega_0\right) - \gamma/2\right] a(\omega) = -\sqrt{\gamma}a_{\text{IN}}(\omega) \ . \tag{3.11}$$

Using eq. (3.9) to get a similar expression for the outgoing field and using it to eliminate $a(t)$ gives the relation between the incoming and outgoing field

$$a_{\text{OUT}}(\omega) = \frac{\gamma/2 + i(\omega - \omega_0)}{\gamma/2 - i(\omega - \omega_0)}a_{\text{IN}}(\omega) \ . \tag{3.12}$$

3.2 Transmission coefficient

Now we want to compute the transmission coefficient for a cavity with two sides that are coupled to the environment, as shown in fig. 3.1. We will consider the situation where the coupling is equal on both sides of the cavity and where only the b fields have a non-zero input b_{IN}. In this case, the equation of motion for the cavity generalizes to

$$\dot{a} = -\frac{i}{\hbar}[H_{\text{sys}}, a] + \frac{\gamma}{2}a(t) + \sqrt{\gamma}\left[a_{\text{IN}}(t) + b_{\text{IN}}(t)\right] \ , \tag{3.13}$$

with the boundary conditions

$$\begin{aligned} a_{\text{IN}}(t) + a_{\text{OUT}}(t) &= \sqrt{\gamma}a(t) \ , \\ b_{\text{IN}}(t) + b_{\text{OUT}}(t) &= \sqrt{\gamma}a(t) \ . \end{aligned} \tag{3.14}$$

Changing equation eq. (3.13) to frequency space and setting $a_{\text{IN}} = 0$ gives

$$a_{\text{OUT}}\left(\omega\right) = \frac{\gamma}{\gamma - i\left(\omega - \omega_0\right)}b_{\text{IN}}\left(\omega\right) \ , \tag{3.15}$$

When performing a transmission experiment the ratio of the output signal to the input signal is given by [22]

$$\left|S\right|^2 = \left|\frac{\gamma}{\gamma - i\left(\omega - \omega_0\right)}\right|^2 \ . \tag{3.16}$$

The transmitted signal is then composed of a sharp peak around the resonance frequency of the cavity $\omega = \omega_0$. The width of this peak is given by the coupling of the cavity to the environment γ. For cavities with losses, the losses would also affect the width of the peaks [22]. Cavity photons interacting with a condensed matter system can have several resonance frequencies corresponding to their effective theory. In this case, the transmission coefficient will have a peak for all the resonances [22].

3.3 Input-output with circular polarization

The effective photon theories that we will encounter in chapter 6, contain terms that mix left and right-handed photons $h_{LR}a_L^\dagger a_R$ and $h_{RL}a_R^\dagger a_L$. In a transmission experiment, these terms open up the possibility of a right-handed input giving rise to a left-handed output and vice versa. In order to describe these processes in the input-output formalism, we must generalize the formalism to include two polarizations of light

$$\begin{aligned} H &= H_{\text{sys}} + \sum_{i\in \text{L,R}} H^i_{\text{B}} + H^i_{\text{int}} \ , \\ H^i_{\text{B}} &= \hbar \int d\omega b_i^\dagger(\omega) b_i(\omega) \ , \\ H^i_{\text{int}} &= i\hbar \int d\omega g \left(b_i(\omega) a_i^\dagger - a_i b_i^\dagger(\omega) \right) \ , \\ H_{\text{sys}} &= \sum_{i,j\in \text{R,L}} h_{ij} a_i^\dagger a_j \ . \end{aligned} \tag{3.17}$$

In this model, both the heat bath and cavity contain left and right-handed photons and the coupling between the cavity and the heat bath conserves the handedness. This model gives the equations of motion

$$\begin{aligned} \dot{a}_i(t) &= -i \sum_j h_{ij} a_j(t) - \frac{\gamma}{2} a_i(t) + \sqrt{\gamma} a_{IN,i}(t) \ , \\ \dot{a}_i(t) &= -i \sum_j h_{ij} a_j(t) + \frac{\gamma}{2} a_i(t) - \sqrt{\gamma} a_{OUT,i}(t) \ . \end{aligned} \tag{3.18}$$

We now want to specialize to the case where only one of the input fields is non-zero. We start by computing the case where $a_{\text{IN,R}} = 0$, and calculated the relation between $a_{\text{IN,L}}$ and $a_{\text{OUT,R}}$. Starting with the three relevant equations

$$\begin{aligned} \dot{a}_{\text{L}}(t) &= -i \left(h_{\text{LL}} a_{\text{L}}(t) + h_{\text{LR}} a_{\text{R}}(t) \right) - \frac{\gamma}{2} a_{\text{L}}(t) + \sqrt{\gamma} a_{IN,\text{L}}(t) \ , \\ \dot{a}_{\text{R}}(t) &= -i \left(h_{\text{RR}} a_{\text{R}}(t) + h_{\text{RL}} a_{\text{L}}(t) \right) + \frac{\gamma}{2} a_{\text{R}}(t) - \sqrt{\gamma} a_{\text{OUT,R}}(t) \ , \\ \dot{a}_{\text{R}}(t) &= -i \left(h_{\text{RR}} a_{\text{R}}(t) + h_{\text{RL}} a_{\text{L}}(t) \right) - \frac{\gamma}{2} a_{\text{R}}(t) \ , \end{aligned} \tag{3.19}$$

and transforming to frequency space gives

$$\begin{aligned} \left(i h_{\text{LL}} - i\omega + \frac{\gamma}{2} \right) a_{\text{L}}(\omega) + i h_{\text{LR}} a_{\text{R}}(\omega) &= \sqrt{\gamma} a_{\text{IN,L}}(\omega) \ , \\ \left(i h_{\text{RR}} - i\omega - \frac{\gamma}{2} \right) a_{\text{R}}(\omega) + i h_{\text{RL}} a_{\text{L}}(\omega) &= -\sqrt{\gamma} a_{\text{OUT,R}}(\omega) \ , \\ \left(i h_{\text{RR}} - i\omega + \frac{\gamma}{2} \right) a_{\text{R}}(\omega) + i h_{\text{RL}} a_{\text{L}}(\omega) &= 0 \ . \end{aligned} \tag{3.20}$$

Solving the equation gives

$$a_{\text{OUT,R}}(\omega) = \frac{\gamma i h_{\text{RL}}}{-\left(i h_{\text{LL}} - i\omega + \frac{\gamma}{2} \right) \left(i h_{\text{RR}} - i\omega + \frac{\gamma}{2} \right) - |h_{\text{RL}}|^2} a_{\text{IN,L}}(\omega) \ , \tag{3.21}$$

where we have used the fact that $h_{\mathrm{RL}}^* = h_{\mathrm{LR}}$ for a Hermitian Hamiltonian. By an analogous calculation, the coefficient for transforming the handedness from right to left is

$$a_{\mathrm{OUT,L}}(\omega) = \frac{\gamma i h_{\mathrm{LR}}}{-\left(ih_{\mathrm{LL}} - i\omega + \frac{\gamma}{2}\right)\left(ih_{\mathrm{RR}} - i\omega + \frac{\gamma}{2}\right) - |h_{\mathrm{RL}}|^2} a_{\mathrm{IN,R}}(\omega) \tag{3.22}$$

Since the transmission coefficient equals the absolute value of this prefactor and that $h_{\mathrm{LR}} = h_{\mathrm{RL}}^*$, the transmission from right to left equals the transmission from left to right. These processes are therefore symmetric between left and right-handed photons and can not detect dichroism. The conclusion of this chapter is therefore that detecting dichroism in an input-output experiment requires the left and right-handed photon bands to have different dispersions.

Chapter 4

Functional integration methods

The functional integral formalism is a powerful formulation of quantum field theory. In quantum field theory, the functional path integral is used to calculate correlators between fields [2]. In condensed matter physics, the statistical partition function can be formulated as a path integral [10]. The formalism has the advantage of replacing operators with numbers. In the bosonic case, the operators get replaced with complex numbers and in the fermionic case, they become anticommuting Grassmann numbers. The use of numbers avoids complicated combinatorial arguments. Another advantage of the functional integral formalism is that it simplifies the construction of effective field theories [10, 37].

This chapter presents relevant topics in the functional integral formalism, which will be applied in chapter 6. In the first section, the functional field integral for the quantum partition function is introduced. The frequency representation of the field integral is also discussed. In the following sections, functional Gaussian integration and a method to determine renormalized dispersions are introduced. These techniques are useful for constructing and analyzing effective field theories. For an in-depth introduction to the topic, a good source is Altland and Simon [10].

4.1 Field integral for quantum partition function

In thermal equilibrium, much of the information about a physical system is given by the partition function

$$\mathcal{Z} = \mathrm{tr}\left\{ e^{-\beta\left(\hat{H}-\mu\hat{N}\right)} \right\} = \sum_n \langle n|\, e^{-\beta\left(\hat{H}-\mu\hat{N}\right)}\, |n\rangle \ . \tag{4.1}$$

Here $\beta = \hbar/k_B T$, k_B is the Boltzmann constant, T is the temperature of the system, $\hat{H}$ is the Hamiltonian of the system, μ is the chemical potential, $\hat{N}$ is the number operator and the sum goes over all possible states of the system $|n\rangle$.

For problems with a large number or infinite degrees of freedom, it is convenient to rewrite the partition function as a path integral [10]. The path integral is constructed in an analogous way to the path integral for correlators in quantum mechanics, by noting that the propagator in quantum mechanics $e^{-it\hat{H}/\hbar}$ becomes the statistical weight function $e^{-\beta\hat{H}}$, when evaluating at the imaginary time $t = -i\beta$. Details of the derivation are given in [10]. Written as a path integral, the partition function becomes

$$Z = \int_{\psi(0)=\pm\psi(\beta)} D(\psi^\dagger, \psi) e^{-S[\psi^\dagger,\psi]/\hbar} \,, \tag{4.2}$$

where $\psi^\dagger$ and ψ are the bosonic or fermionic fields, $D(\psi^\dagger, \psi)$ is the functional integral measure, and the action is given by

$$S[\psi^\dagger, \psi] = \int_0^\beta d\tau \left[\psi^\dagger \partial_\tau \psi + H(\psi^\dagger, \psi) - \mu N(\psi^\dagger, \psi)\right] \,.$$

For bosonic fields, the ψ and $\psi^\dagger$ fields are complex numbers and ψ is periodic $\psi(\beta) = +\psi(0)$. Fermionic fields are Grassman numbers, and ψ is anti-periodic $\psi(\beta) = -\psi(0)$.

We now apply this general procedure to constructing the path integral representation of the Hamiltonian given in eq. (2.13), with H_{int} given by eq. (2.16). This Hamiltonian describes the interaction between an electromagnetic cavity and an electronic system. The Hamiltonian contains both bosonic photon operators and fermionic electron operators. The partition function is then written as a path integral over the bosonic fields $a^\dagger$ and a and the fermionic fields $C^\dagger$ and C

$$Z = \int_{C(0)=-C(\beta)} D(C^\dagger, C) \int_{a(0)=+a(\beta)} D(a^\dagger, a) e^{-S[C^\dagger, C, a^\dagger, a]/\hbar} \,. \tag{4.3}$$

We note that the fermionic electron fields are anti-periodic $C(\tau = 0) = -C(\tau = \beta)$, while the bosonic photon fields are periodic $a(\tau = 0) = a(\tau = \beta)$.

The action in eq. (4.3) is given by

$$\begin{aligned} &S[C^\dagger, C, a^\dagger, a] = \\ &\int_0^\beta d\tau \Big[\sum_{\mathbf{q}l} a^\dagger_{\mathbf{q}\tau l} \left(\hbar\partial_\tau + \hbar\omega_{\mathbf{q}}\right) a_{\mathbf{q}\tau l} + \sum_{\mathbf{k}\sigma\sigma'} C^\dagger_{\mathbf{k}\tau\sigma} \left(\hbar\partial_\tau + \epsilon_{\mathbf{k}\sigma\sigma'}\right) C_{\mathbf{k}\tau\sigma'} \\ &+ \sum_{\mathbf{k}\mathbf{k}'\sigma\sigma' l} g^{\mathbf{k}\mathbf{k}'}_{\sigma\sigma' l} C^\dagger_{\mathbf{k}\tau\sigma} C_{\mathbf{k}'\tau\sigma'} \left(a_{\mathbf{k}-\mathbf{k}',\tau l} + a^\dagger_{\mathbf{k}'-\mathbf{k},\tau-l}\right) \Big] \,. \end{aligned} \tag{4.4}$$

It is convenient to rewrite this action as a frequency representation. In order to change representation, we introduce the Fourier-transformed fields. In the frequency representation, the photon fields are given by

$$a_{\mathbf{q}\tau l} = \frac{1}{\sqrt{\beta}} \sum_n a_{ql} e^{-i\Omega_n \tau} \,,\; a_{ql} = \frac{1}{\sqrt{\beta}} \int_0^\beta d\tau a_{\mathbf{q}\tau l} e^{i\Omega_n \tau} \,, \tag{4.5}$$

where $n \in \mathbb{Z}$, $\Omega_n = 2n\pi/\beta$ and $q = (-i\Omega_n, \mathbf{q})$. Similarly, the electron fields are given by

$$C_{\mathbf{k}\tau\sigma} = \frac{1}{\sqrt{\beta}} \sum_n C_{k\sigma} e^{-i\omega_n \tau} \ , \ C_{k\sigma} = \frac{1}{\sqrt{\beta}} \int_0^\beta d\tau C_{\mathbf{k}\tau\sigma} e^{i\omega_n \tau} \ , \tag{4.6}$$

where $n \in \mathbb{Z}$, $\omega_n = (2n+1)\,\pi/\beta$ and $k = (-i\omega_n, \mathbf{k})$. The definition of Ω_n and ω_n ensure that the periodic/anti-periodic boundary conditions are fulfilled. Using eq. (4.5) and eq. (4.6), we can rewrite eq. (4.4)

$$\begin{aligned} S[C^\dagger, C, a^\dagger, a] = &\sum_{ql} \left(-i\hbar\Omega_n + \hbar\omega_{\mathbf{q}}\right) a^\dagger_{ql} a_{ql} + \sum_{k\sigma\sigma'} \epsilon_{k\sigma\sigma'} C^\dagger_{k\sigma} C_{k\sigma'} \\ &+ \sum_{kk'\sigma\sigma' l} \frac{g^{\mathbf{k}\mathbf{k}'}_{\sigma\sigma' l}}{\sqrt{\beta}} C^\dagger_{k\sigma} C_{k'\sigma'} \left(a_{k-k'l} + a^\dagger_{k'-k-l}\right) \ . \end{aligned} \tag{4.7}$$

In the last line we defined $k' = \left(-i\omega_{n'}, \mathbf{k}'\right)$, $\epsilon_{k\sigma\sigma'} = -i\hbar\omega_n + \epsilon_{\mathbf{k}\sigma\sigma'}$ and used the identity $\int_0^\beta d\tau e^{-i(x-x')\tau} = \beta\delta_{xx'}$. The action given in eq. (4.7) will be the starting point when constructing effective photon theories in section 4.3 and chapter 6. To construct effective photon theories, we will utilize Gaussian integrals. The next section is therefore devoted to giving a brief introduction to this topic.

4.2 Gaussian integration

One of the most powerful and useful tools in the functional integral formalism is the Gaussian integral. Gaussian integrals can be used to flexibly construct effective theories of a single field in a system where several fields are present. The effective theory is constructed by integrating out the unwanted fields using Gaussian integrals. Examples of such effective theories will be given in chapter 6.

For a complex boson field v, the Gaussian integral formula becomes [10]

$$\int D(\mathrm{v}^\dagger, \mathrm{v}) e^{-\mathrm{v}^\dagger A \mathrm{v} + \mathrm{w}^\dagger \cdot \mathrm{v} + \mathrm{v}^\dagger \cdot \mathrm{w}} = \frac{1}{\det\{A\}}\, e^{\mathrm{w}^\dagger A^{-1} \mathrm{w}} \ , \tag{4.8}$$

where A is a postivie operator and w is a arbitrary function. For a fermion field ϕ, the Gaussian integral formula reads [10]

$$\int D(\phi^\dagger, \phi) e^{-\phi^\dagger A \phi + \eta^\dagger \cdot \phi + \phi^\dagger \cdot \eta} = \det\{A\}\, e^{\eta^\dagger A^{-1} \eta} \ , \tag{4.9}$$

where η is an arbitrary function. The determinant in eqs. (4.8) and (4.9) is usually not analytically soluble. To approximate the expression for the determinant, the following identity is often useful

$$\det\{A\}^\zeta = e^{\zeta \,\mathrm{Tr}\{\ln A\}} \ . \tag{4.10}$$

This identity will be applied in the next section when deriving an effective photon theory.

4.3 Renormalized spectrum

An application of the path integral formalism is to calculate the renormalized spectrum of one field when it is interacting with other fields. For specificity, we calculate the renormalized spectrum of the right-handed photon fields $a_{\mathrm{R}}^\dagger$ and a_{R} in eq. (4.7) when they are interacting with electron fields $C^\dagger$ and C. We also take the electronic system to be a free electron gas

$$\epsilon_{k\sigma\sigma'} = \epsilon_k \delta_{\sigma\sigma'} = -i\omega_n + \frac{\hbar^2 \mathbf{k}^2}{2m_e} - \mu \, . \tag{4.11}$$

Using eq. (4.11) and rewriting eq. (4.7) gives the action

$$S[C^\dagger, C, a^\dagger, a] = \sum_{ql} \left(-i\hbar\Omega_n + \hbar\omega_{\mathbf{q}}\right) a_{ql}^\dagger a_{ql} + \sum_{kk'\sigma\sigma'} \left[\mathcal{G}^{-1}\right]_{\sigma\sigma'}^{kk'} C_{k\sigma}^\dagger C_{k'\sigma'} \, . \tag{4.12}$$

In the last line, we defined

$$\left[\mathcal{G}^{-1}\right]_{\sigma\sigma'}^{kk'} = \epsilon_k \delta_{kk'} \delta_{\sigma\sigma'} + \sum_l \frac{g_{\sigma\sigma' l}^{\mathbf{k}\mathbf{k}'}}{\sqrt{\beta}} \left(a_{k-k'l} + a_{k'-k-l}^\dagger\right) \, . \tag{4.13}$$

We can now construct an effective photon theory by integrating out the electron fields using the Gaussian integral formula given in eq. (4.9). Performing this integral gives the action

$$S_{\mathrm{eff}} = \sum_{ql} \left(-i\hbar\Omega_n + \hbar\omega_{\mathbf{q}}\right) a_{ql}^\dagger a_{ql} + \mathrm{Tr}\left\{\ln \mathcal{G}^{-1}\right\} \, , \tag{4.14}$$

where the trace is over the momentum and spin indices. To continue with this expression analytically, we assume that the coupling $g_{\sigma\sigma' l}^{\mathbf{k}\mathbf{k}'}$ is small and expand the logarithm. The first-order terms contain only one photon field $a^\dagger$ or a. Momentum and energy conservation restrict the fields to having $q = 0$, giving rise to a space- and time-independent vector potential. Such a vector potential does not have physical meaning, since it does not give rise to electric or magnetic fields. We therefore only include the second-order contribution of the expansion

$$\begin{aligned} S_{\mathrm{eff}} \approx & \sum_{ql} \left(-i\hbar\Omega_n + \hbar\omega_{\mathbf{q}}\right) a_{ql}^\dagger a_{ql} \\ & - \frac{1}{2\beta} \sum_{qk'\sigma\sigma' ll'} \epsilon_{k'+q} \epsilon_{k'} g_{\sigma\sigma' l}^{(\mathbf{k}'+\mathbf{q})\mathbf{k}'} g_{\sigma'\sigma l'}^{\mathbf{k}'(\mathbf{k}'+\mathbf{q})} \left(a_{ql} + a_{-q-l}^\dagger\right) \left(a_{-ql'} + a_{q-l'}^\dagger\right) \, . \end{aligned} \tag{4.15}$$

In the last line we defined the relative coordinate $q = k - k' := (-i\Omega_n, \mathbf{q})$. The second-order contribution to the effective action is depicted diagrammatically in fig. 4.1.

We have now successfully constructed the effective photon theory. The action in eq. (4.15) contains terms that mix left and right-handed photons. To calculate the renormalized spectrum of only right-handed photons, we need the effective

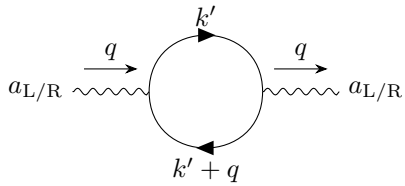

Figure 4.1: Second order correction to photon propagator given by photon-electron interaction.

theory of the right-handed photons. In order to get this effective theory, we must integrate out the left-handed photons using eq. (4.8). We will discuss this step in section 6.1. For the present discussion, it suffices to know that to second order in the coupling constant $g^{\mathbf{k}\mathbf{k}'}_{\sigma\sigma' l}$, the effective theory for right-handed photons becomes

$$S = \sum_q \left(-i\hbar\Omega_n + \hbar\omega_{\mathbf{q}} + \Sigma\left(\mathbf{q}, i\Omega_n\right)\right) a^\dagger_{q\mathrm{R}} a_{q\mathrm{R}} \,. \tag{4.16}$$

The exact expression for $\Sigma\left(\mathbf{q}, i\Omega_n\right)$ is not important for the present discussion and will be given in section 6.1. The new spectrum of the right-handed photons is given by the solutions of the equation

$$-\hbar\omega - i\delta + \hbar\omega_{\mathbf{q}} + \Sigma\left(\mathbf{q}, \omega + i\delta/\hbar\right) = 0 \,, \tag{4.17}$$

which is related to the action by the analytic continuation $i\Omega_n \to \omega + i\delta/\hbar$, where $\delta = 0^+$ [10]. There can be several solutions to eq. (4.17), corresponding to the resonances of the quasiparticles in the system that include the original photon mode a_q [27]. In the second quantized formulation of quantum field theory, acquiring the quasiparticle spectrum would require an explicit diagonalization of the system. For complex systems, an explicit diagonalization can be intractable [27]. This method, therefore, highlights an advantage of the functional integral formalism.

Taking the inverse of eq. (4.17) gives the renormalized Greens function for the cavity photons

$$\mathcal{G}(\omega) = \frac{1}{-i\delta - \hbar\omega + \hbar\omega_{\mathbf{q}} + \Sigma\left(\mathbf{q}, \omega + i\delta/\hbar\right)} \,. \tag{4.18}$$

Plotting eq. (4.18) against the frequency gives resonances for the solutions of eq. (4.17). This is a practical way to solve eq. (4.17) numerically. The resonance frequencies of the Greens function equals the resonance frequency in a transmission experiment given by eq. (3.16). However, the amplitude of the transmission coefficient would be different. With the amplitude in a transmission experiment being determined by the coupling of the cavity to the environment, the losses in the cavity and the losses in the condensed matter system [22].

Chapter 5

Superconductivity

The goal of this chapter is to introduce time-reversal symmetry-breaking triplet superconductors. In order to describe triplet superconductors, we introduce the **d**-vector formalism. This formalism describes superconducting correlations in terms of a three-dimensional vector quantity. Using the **d**-vector formalism, we present the time-reversal symmetry-breaking states which will be studied in the following chapter.

5.1 Mean-field action

In mean-field, a general superconductor is described by the action

$$S = \sum_{k\sigma} \epsilon_{k\sigma} C^\dagger_{k\sigma} C_{k'\sigma} + \frac{1}{2} \sum_{k\sigma\sigma'} \left(C^\dagger_{k\sigma} C^\dagger_{-k\sigma'} \Delta_{\sigma'\sigma}(k) + \bar{\Delta}_{\sigma\sigma'}(k) C_{-k\sigma'} C_{k\sigma} \right) . \quad (5.1)$$

Starting with the last term in eq. (5.1), using the fact that the electron fields anticomute and relabeling the summation variables $k \to -k$ and $\sigma, \sigma' \to \sigma', \sigma$ gives the symmetry requirement $\Delta_{\sigma',\sigma}(k) = -\Delta_{\sigma,\sigma'}(-k)$ [10]. The gap parameter $\Delta_{\sigma\sigma'}(k)$ must then be odd under the total transformation of interchanging the spins $\sigma, \sigma' \to \sigma', \sigma$, and reversing the frequency $i\omega_n \to -i\omega_n$ and the momentum $\mathbf{k} \to -\mathbf{k}$. Considering frequency-independent gap parameters gives two possibilities, the gap parameter can be even in momentum and odd in spin or vice versa. It is therefore useful to divide the gap parameter into a triplet which is even under the interchange of spin and a singlet which is odd. This will be done in the next section using the **d**-vector formalism.

5.2 d-vector formalism

Converting eq. (5.1) to a Nambu spinor representation gives

$$S = \frac{1}{2} \sum_{kk'} \bar{\Psi}_k \mathcal{G}^{-1}_{kk'} \Psi_{k'} , \quad (5.2)$$

with

$$\mathcal{G}^{-1}_{kk'} = \begin{bmatrix} \epsilon_\uparrow(k) & 0 & \Delta_{\uparrow\uparrow}(k) & \Delta_{\downarrow\uparrow}(k) \\ 0 & \epsilon_\downarrow(k) & \Delta_{\uparrow\downarrow}(k) & \Delta_{\downarrow\downarrow}(k) \\ \bar{\Delta}_{\uparrow\uparrow}(k) & \bar{\Delta}_{\uparrow\downarrow}(k) & -\epsilon_\uparrow(-k) & 0 \\ \bar{\Delta}_{\downarrow\uparrow}(k) & \bar{\Delta}_{\downarrow\downarrow}(k) & 0 & -\epsilon_\downarrow(-k) \end{bmatrix} \delta_{kk'} \,, \tag{5.3}$$

where we have defined the Nambu spinor

$$\Psi_k = \begin{bmatrix} C_{k,\uparrow} \\ C_{k,\downarrow} \\ C^\dagger_{-k,\uparrow} \\ C^\dagger_{-k,\downarrow} \end{bmatrix} \,. \tag{5.4}$$

We now write the matrix of gap parameters in terms of the **d**-vector [12, 40]

$$\begin{bmatrix} \Delta_{\uparrow\uparrow}(k) & \Delta_{\uparrow\downarrow}(k) \\ \Delta_{\downarrow\uparrow}(k) & \Delta_{\downarrow\downarrow}(k) \end{bmatrix} = i\left(d_0(k) + \mathbf{d}(k)\cdot\hat{\boldsymbol{\sigma}}\right)\hat{\sigma}_y \,, \tag{5.5}$$

where $\hat{\boldsymbol{\sigma}}$ is the vector of Pauli matrices $d_0(k) = \Delta^S_{\uparrow,\downarrow}(k)$ and

$$\mathbf{d}(k) = \frac{1}{2}\begin{bmatrix} \Delta^T_{\downarrow\downarrow}(k) - \Delta^T_{\uparrow\uparrow}(k) \\ -i\left(\Delta^T_{\downarrow\downarrow}(k) + \Delta^T_{\uparrow\uparrow}(k)\right) \\ 2\Delta^T_{\uparrow\downarrow}(k) \end{bmatrix} \,, \tag{5.6}$$

where the superscripts S and T denote the singlet and triplet states respectively. One of the advantages of this formalism is that $\mathbf{d}(k)$ transforms as a vector under spin rotations. The average spin of the Cooper pair is given by $\langle S_k\rangle = i\left(\mathbf{d}(k)\times\mathbf{d}^*(k)\right)$. A cooper pair with a preferred spin direction is associated with a magnetic field. As discussed in section 2.6, a magnetic field breaks time-reversal symmetry. Therefore, if $i\left(\mathbf{d}(k)\times\mathbf{d}^*(k)\right) \neq 0$ the Cooper pairs break time-reversal symmetry and are characterized as non-unitary. However, as we will see in the next section, states with $i\left(\mathbf{d}(k)\times\mathbf{d}^*(k)\right) = 0$ can also break time-reversal symmetry.

5.3 Time-reversal symmetry breaking

In this master thesis, we will consider three p-wave gap parameters that break time-reversal symmetry. In order to simplify the discussion we specialize to states that are compatible with a tetragonal lattice structure with a cylindrical Fermi surface [12]. The gap parameters considered in this thesis are not meant to exhaust the possible time-reversal symmetry-breaking states, but to analyze if time-reversal symmetry breaking in the gap parameter can lead to dichroism.

The simplest time-reversal symmetry-breaking state is given by the **d**-vector

$$\mathbf{d}(k) = \left(\hat{x} + i\hat{y}\right)\left(k_x + ik_y\right)/|\mathbf{k}| \,, \tag{5.7}$$

or written as a matrix

$$i\left(\mathbf{d}\cdot\hat{\boldsymbol{\sigma}}\right)\hat{\sigma}_y = \begin{bmatrix} \Delta_0\left(k_x + k_y\right) & 0 \\ 0 & 0 \end{bmatrix} \,. \tag{5.8}$$

In this state, only the spin-up band is superconducting. With all the Cooper pairs being spin up, the state is non-unitary. The next state we consider is also non-unitary and is given by the **d**-vector $\mathbf{d}(k) = \hat{x}k_x + i\hat{y}k_y$, which corresponds to the matrix

$$i\left(\mathbf{d}\cdot\hat{\boldsymbol{\sigma}}\right)\hat{\sigma}_y = \begin{bmatrix} -\Delta^0\left(k_x + k_y\right) & 0 \\ 0 & \Delta^0\left(k_x - k_y\right) \end{bmatrix}. \tag{5.9}$$

In both the preceding states, the time-reversal symmetry breaking occurred in the spin part of the action. However, the time-reversal symmetry breaking can also occur in the orbital part of the gap parameter. One such example, is described by the **d**-vector $\mathbf{d}(k) = \left(k_x + ik_y\right)\hat{z}$, or written as a matrix

$$i\left(\mathbf{d}\cdot\hat{\boldsymbol{\sigma}}\right)\hat{\sigma}_y = \begin{bmatrix} 0 & \Delta_0\left(k_x + ik_y\right) \\ \Delta_0\left(k_x + ik_y\right) & 0 \end{bmatrix}. \tag{5.10}$$

This gap function is an example of a topological chiral state, meaning that the phase changes by $\pm 2\pi$ as $\mathbf{k}$ follows a closed path around the Fermi surface [3, 19]. Since the **d**-vector only has one component, $\mathbf{d}\times\mathbf{d}^* = 0$ and the state is unitary. Under time reversal, the state transforms to $\mathbf{d} = -\left(k_x - ik_y\right)\hat{z}$ [3] and is therefore not invariant. This state was a leading candidate for the gap symmetry of strontium ruthenate [12], but later experiments have cast doubts on this claim [41].

Chapter 6

Circular dichroism in cavity systems

In this chapter, we analyze if interactions between electromagnetic cavities and electronic systems can give rise to circular dichroism in a transmission experiment. In the first section, we derive a general condition for when an effective photon theory can give rise to circular dichroism. This condition is used in the following sections to analyze possible circular dichroism in a ferromagnetic metal, ferromagnetic superconductor, and the superconductors discussed in chapter 5.

6.1 Effective theory for one polarization

As discussed in chapter 3, transmission experiments probe the effective theory of the cavity photons. The goal of this section is to determine the conditions for which an effective photon action will give rise to circular dichroism in a transmission experiment. To aid in the discussion, we consider the effective action calculated in section 4.3. This effective action is calculated for the cavity photons interacting with a normal metal. However, the conclusion of this section is independent of the specific electronic system.

The contribution to the effective photon action S_{eff} from the electron-photon interaction is given by eq. (4.15)

$$S_{\text{eff}}^{e-p} = -\frac{1}{2\beta} \sum_{qk'\sigma\sigma' ll'} \epsilon_{k'+q}\epsilon_{k'} g_{\sigma\sigma' l}^{(\mathbf{k}'+\mathbf{q})\mathbf{k}'} g_{\sigma' l'}^{\mathbf{k}'(\mathbf{k}'+\mathbf{q})} \left(a_{ql} + a_{-q-l}^\dagger\right)\left(a_{-ql'} + a_{q-l'}^\dagger\right) . \tag{6.1}$$

The terms in this action can be rearranged into three types

$$\begin{aligned} S_{\text{eff}}^{e-p} = \sum_q \Big[& C_q^{\text{LL}} \left(a_{qL} + a_{-qR}^\dagger\right)\left(a_{-qL} + a_{qR}^\dagger\right) \\ & + C_q^{\text{RR}} \left(a_{qR} + a_{-qL}^\dagger\right)\left(a_{-qR} + a_{qL}^\dagger\right) \\ & + C_q^{\text{LR}} \left(a_{qL} + a_{-qR}^\dagger\right)\left(a_{-qR} + a_{qL}^\dagger\right) \Big] , \end{aligned} \tag{6.2}$$

where we have defined the coefficients

$$
\begin{aligned}
C_q^{\mathrm{LL}} &= -\frac{1}{2\beta}\sum_{k'}\epsilon_{k'+q}\epsilon_{k'}\, g_{\sigma\sigma'\mathrm{L}}^{(\mathbf{k}'+\mathbf{q})\mathbf{k}'}\, g_{\sigma'\sigma\mathrm{L}}^{\mathbf{k}'(\mathbf{k}'+\mathbf{q})} \ , \\
C_q^{\mathrm{RR}} &= -\frac{1}{2\beta}\sum_{k'}\epsilon_{k'+q}\epsilon_{k'}\, g_{\sigma\sigma'\mathrm{R}}^{(\mathbf{k}'+\mathbf{q})\mathbf{k}'}\, g_{\sigma'\sigma\mathrm{R}}^{\mathbf{k}'(\mathbf{k}'+\mathbf{q})} \ , \\
C_q^{\mathrm{LR}} &= -\frac{1}{2\beta}\sum_{k'\sigma\sigma'}\epsilon_{k'+q}\epsilon_{k'}\left(g_{\sigma\sigma'\mathrm{L}}^{(\mathbf{k}'+\mathbf{q})\mathbf{k}'}\, g_{\sigma'\sigma\mathrm{R}}^{\mathbf{k}'(\mathbf{k}'+\mathbf{q})} + g_{\sigma\sigma'\mathrm{R}}^{(\mathbf{k}'-\mathbf{q})\mathbf{k}'}\, g_{\sigma'\sigma\mathrm{L}}^{\mathbf{k}'(\mathbf{k}'-\mathbf{q})}\right) \ .
\end{aligned}
\tag{6.3}
$$

The effective photon actions encountered in the next sections can also be written in the same form as eq. (6.2).

The C_q^{LL}- and C_q^{RR}-terms do not directly contribute to number operators for left or right-handed photons $a_{q,\mathrm{R}}^\dagger a_{q,\mathrm{R}}$ and $a_{q,\mathrm{L}}^\dagger a_{q,\mathrm{L}}$. To leading order, these terms will not contribute to transmission experiments involving a single circular polarization. These terms do include the products of photon fields $a_{q,\mathrm{R}}^\dagger a_{q,\mathrm{L}}$ and $a_{q,\mathrm{R}}^\dagger a_{q,\mathrm{L}}$. These combinations describe processes that transform the polarization of the photon. As discussed in chapter 3, these processes do not give rise to circular dichroism. We will therefore focus on the C_q^{LR}-terms in our discussion of circular dichroism.

The C_q^{LR}-terms contain number operators for left and right handed photons $a_{q,\mathrm{R}}^\dagger a_{q,\mathrm{R}}$ and $a_{q,\mathrm{L}}^\dagger a_{q,\mathrm{L}}$. A transmission experiment involving only one polarization probes the effective theory of that polarization. To leading order, this effective theory is achieved by neglecting the other polarization. These effective theories are

$$
\begin{aligned}
S_{\mathrm{eff,L}}^{e-p} &= \sum_q C_q^{\mathrm{LR}} a_{q\mathrm{L}}^\dagger a_{q,\mathrm{L}} \ , \\
S_{\mathrm{eff,R}}^{e-p} &= \sum_q C_{-q}^{\mathrm{LR}} a_{q\mathrm{R}}^\dagger a_{q,\mathrm{R}} \ .
\end{aligned}
\tag{6.4}
$$

From eq. (6.4) it is clear that to first order in C_q^{LR}, dichroism can only occur when $C_q^{\mathrm{LR}} \neq C_{-q}^{\mathrm{LR}}$. In the dipole approximation $\mathbf{q} = 0$, dichroism relies on C_q^{LR} not being even in the frequency $q_0 = -(i\omega_n - i\omega_{n'}) = -i\Omega_n$. For the coefficients defined in eq. (6.3), $C_q^{\mathrm{LR}} = C_{-q}^{\mathrm{LR}}$. Therefore, interactions with a normal metal do not give rise to circular dichroism. This fact also follows from the time-reversal symmetry of a normal metal.

In the next section, we consider if interactions with a ferromagnetic metal will give rise to circular dichroism. A ferromagnetic metal is a simple time-reversal symmetry-breaking system, making it an ideal system to test the method which has been developed in this section and in chapter 4. The ferromagnetic metal is also a good precursor to the ferromagnetic superconductor which will be discussed in section 6.3.

6.2 Ferromagnetic metal

A ferromagnetic metal is described as a free electron gas with spin-split bands. The spin split bands give the ferromagnet a net magnetization which breaks

time-reversal symmetry. The ferromagnet is placed at the bottom of the cavity and interacts with the cavity modes through the Zeeman interaction eq. (2.26). The action describing this setup is

$$\begin{aligned} S = &\sum_{k,\sigma} \left(-i\hbar\omega_n + \epsilon_{\mathbf{k}\sigma} - \mu\right) C^\dagger_{k\sigma} C_{k\sigma} \\ &+ \sum_{q,l} \left(-i\hbar\Omega_n + \omega_{\mathbf{q}}\right) a^\dagger_{ql} a_{ql} \\ &+ \sum_{kk'\sigma\sigma' l} \frac{g^{k'-k}_{\sigma\sigma' s}}{\sqrt{\beta}} \left(a_{k'-kl} + a^\dagger_{k-k'-l}\right) C^\dagger_{k\sigma} C_{k'\sigma'} \ , \end{aligned} \tag{6.5}$$

where $l \in \{L, R\}$, $g^{k'-k}_{\sigma\sigma' l}$ is given by eq. (2.25) and $\epsilon_{\mathbf{k},\uparrow,} = \epsilon_{\mathbf{k},\downarrow} - h$, where h is the spin splitting. The system can be described more compactly in terms of the spinor $\Psi_k = \begin{pmatrix} C_{k,\uparrow} & C_{k,\downarrow} \end{pmatrix}^T$

$$S = \sum_{ql} \left(-i\Omega_n + \omega_{\mathbf{q}}\right) a^\dagger_{al} a_{ql} + \sum_{kk'} \Psi^\dagger_k [\mathcal{G}^{-1}]_{kk'} \Psi_{k'} \ , \tag{6.6}$$

with $[\mathcal{G}^{-1}]_{kk'} = [\mathcal{G}_0^{-1}]_{kk'} + \chi_{kk'}$,

$$[\mathcal{G}_0^{-1}]_{kk'} = \begin{bmatrix} \epsilon_\uparrow(k) & 0 \\ 0 & \epsilon_\downarrow(k) \end{bmatrix} \delta_{k,k'} \ , \tag{6.7}$$

and

$$\chi_{kk'} = \tilde{g}_z \begin{bmatrix} 0 & -\left(a_{k'-k\mathrm{L}} + a^\dagger_{k-k'\mathrm{R}}\right) e^{-i\phi} \\ \left(a_{k'-k\mathrm{R}} + a^\dagger_{k-k'\mathrm{L}}\right) e^{i\phi} & 0 \end{bmatrix} . \tag{6.8}$$

Integrating out the electron fields and expanding the resulting logarithm to second order gives

$$S_{\text{eff}} \approx \sum_{q,l} \left(-i\Omega_n + \omega_{\mathbf{q}}\right) a^\dagger_{a,l} a_{q,l} - \frac{1}{2} \operatorname{Tr}\left\{ \left(\mathcal{G}_0 \chi\right)^2 \right\} , \tag{6.9}$$

Using these expressions we can calculate the contribution to the effective photon action, from the interaction with the electrons

$$\begin{aligned} S^{e-p}_{\text{eff}} &= -\frac{1}{2} \operatorname{Tr}\left\{ \left(\mathcal{G}_0 \chi\right)^2 \right\} \\ &= -\tilde{g}_z^2 \sum_{k,k'} \left(a_{k-k'\mathrm{L}} + a^\dagger_{k'-k\mathrm{R}}\right) \left(a_{k'-k\mathrm{R}} + a^\dagger_{k-k'\mathrm{L}}\right) \frac{1}{\epsilon_\uparrow(k)\, \epsilon_\downarrow(k')} \\ &= -\tilde{g}_z^2 \sum_{\mathbf{q}} \left(a_{q\mathrm{L}} + a^\dagger_{-q\mathrm{R}}\right) \left(a_{-q\mathrm{R}} + a^\dagger_{q\mathrm{L}}\right) \\ &\times \sum_{\mathbf{k'}n'} \frac{1}{\left(-i\hbar\omega_{n'} - i\hbar\Omega_n + \epsilon_{\uparrow,\mathbf{k'}+\mathbf{q}}\right) \left(-i\hbar\omega_{n'} + \epsilon_{\downarrow,\mathbf{k'}}\right)} \ . \end{aligned} \tag{6.10}$$

Using the notation from the previous section we have

$$\begin{aligned} C_q^{LR} &= -\tilde{g}_z^2 \sum_{\mathbf{k'}n'} \frac{1}{\left(-i\hbar\omega_{n'} - i\hbar\Omega_n + \epsilon_{\uparrow,\mathbf{k'}+\mathbf{q}}\right)\left(-i\hbar\omega_{n'} + \epsilon_{\downarrow,\mathbf{k'}}\right)} \\ &= -\tilde{g}_z^2 \sum_{\mathbf{k'}} \left[\frac{n_{\mathrm{F}\uparrow}\left(\mathbf{k'}+\mathbf{q}\right)}{i\hbar\Omega_n - \epsilon_{\uparrow,\mathbf{k'}+\mathbf{q}} + \epsilon_{\downarrow,\mathbf{k'}}} + \frac{n_{\mathrm{F}\downarrow}\left(\mathbf{k'}\right)}{-\epsilon_{\downarrow,\mathbf{k'}} - i\hbar\Omega_n + \epsilon_{\uparrow,\mathbf{k'}+\mathbf{q}}} \right] . \end{aligned} \tag{6.11}$$

In the last line, we computed the Matsubara sum over $\omega_{n'}$ and introduced the Fermi-Dirac distribution $n_{\mathrm{F}\sigma}\left(\mathbf{k}\right) = 1/\left(e^{\beta\epsilon_{\mathbf{k}\sigma}}+1\right)$. We now take the dipole approximation by setting $\mathbf{q}=0$. In the dipole approximation one assumes that $\mathbf{q} \ll \mathbf{k}_{\mathrm{F}}$, where $\mathbf{k}_{\mathrm{F}}$ is the Fermi wave-vector. Taking the dipole approximation and using $\epsilon_{\mathbf{k'},\uparrow,} = \epsilon_{\mathbf{k'},\downarrow} - h$ gives

$$\begin{aligned} C^{\mathrm{LR}}_{i\Omega_n} &= -\tilde{g}_z^2 \sum_{\mathbf{k'}} \frac{n_{\mathrm{F},\uparrow}\left(\mathbf{k'}\right) - n_{\mathrm{F},\downarrow}\left(\mathbf{k'}\right)}{i\hbar\Omega_n + h} \\ &= -\tilde{g}_z^2 \frac{\beta\delta N}{i\hbar\Omega_n + h} , \end{aligned} \tag{6.12}$$

where we have defined

$$\delta N = \sum_{\mathbf{k'}} n_{\mathrm{F},\uparrow}\left(\mathbf{k'}\right) - n_{\mathrm{F},\downarrow}\left(\mathbf{k'}\right) . \tag{6.13}$$

At zero temperature, the constant becomes $\delta N = \frac{A_{\mathrm{FM}} m_e h}{2\pi\hbar^2}$, where A_{FM} is the area of the ferromagnet.

Using eq. (6.4) the effective action for the left/right-handed modes can be computed

$$S^l_{\mathrm{eff}} = \sum_{i\Omega_n} \left[-i\hbar\Omega_n + \hbar\omega_0 - \tilde{g}_z^2 \delta N \frac{1}{i\hbar\Omega_n s_l + h} \right] a^\dagger_{(-i\Omega_n,0)l} a_{(-i\Omega_n,0)l} , \tag{6.14}$$

where $s_{\mathrm{L}} = 1$ and $s_{\mathrm{R}} = -1$. Using eq. (4.17), the renormalized photon dispersion is given by the solutions of the equation

$$-i\delta - \hbar\omega + \hbar\omega_{\mathbf{q}} - \frac{Ch}{s_l\hbar\omega + s_l\hbar i\delta + h} = 0 . \tag{6.15}$$

In the last line, we performed the analytic continuation $i\Omega_n = \omega + i\delta/\hbar$ and defined the constant $C = \tilde{g}_z^2 \delta N/h$. This equation has the solution

$$\omega = \frac{\omega_{\mathbf{q}}}{2} + s_l \frac{h}{2\hbar} \pm \frac{s_l}{2}\sqrt{\left(s_l\omega_{\mathbf{q}} + h/\hbar\right)^2 - 4Chs_l/\hbar^2} . \tag{6.16}$$

In the zero temperature limit, the constant becomes

$$C = \frac{\mu_B^2 m_e}{\pi L_z \epsilon_0 c^2 \hbar^2}\hbar\omega_0 = 2.82 \cdot 10^{-15}\mathrm{m}/L_z\hbar\omega_0 . \tag{6.17}$$

In the last equality, we expressed the constant in terms of $\hbar\omega_0 = \hbar c\frac{\pi}{L_z}$ and inserted the value for the Bohr magneton μ_{B}, electron mass m_e, vacuum permeability ϵ_0 and the speed of light c. For a realistic cavity size L_z, the coupling is too small to be detected.

There are several ways to enhance the coupling. First, we will consider the effect of giving the ferromagnetic metal a finite thickness. Assuming that the magnetic field is approximately constant across the ferromagnetic metal, the only effect of considering a finite thickness is to increase the difference in occupation between spin up and spin down electrons given by eq. (6.13) [21, 37]. Calculating δN for a three-dimensional free electron gas gives

$$\delta N^{\mathrm{3D}} = \frac{2\sqrt{2}}{3\pi}\frac{\alpha L_z\sqrt{m_e}}{\hbar}\frac{(\mu+h)^{3/2}-\mu^{3/2}}{h}\delta N^{\mathrm{2D}} \,, \tag{6.18}$$

where we have written δN^{3D} in terms of the two dimensional electron gas $\delta N^{\mathrm{2D}} = \frac{A_{\mathrm{FM}} m_e}{2\pi\hbar^2}$. The ratio between the ferromagnetic metal's thickness and the cavity's width L_z is denoted by α. From eq. (2.2), it is clear that the z-dependence of the magnetic field is given by $\cos \pi z/L_z$. At $z = 0$ the magnetic field is therefore at a maximum and we can set $\alpha = 0.1$, which only gives a five percent change in the magnetic field across the ferromagnetic metal. This gives the coupling

$$C = \frac{\sqrt{2}\alpha\mu_B^2 m_e^{3/2}\sqrt{\mu}}{\epsilon_0 c^2\hbar^3}\hbar\omega_0 = 5.70\cdot 10^{-7}\hbar\omega_0 \,, \tag{6.19}$$

where we have assumed $\mu \ll h$ and set $\mu = 1\,\mathrm{eV}$. The coupling could be increased further if the effective electron mass was higher than the free electron mass or if the chemical potential was larger than $\mu = 1\,\mathrm{eV}$. In addition to increasing the coupling strength, we can enhance the effect of the ferromagnetic metal by tuning the resonance frequency of the cavity to equal the spin-splitting, $\hbar\omega_0 = h$.

The amplitude of the resonance is given by the absolute value of the Green's function eq. (3.16) and becomes

$$|\mathcal{G}(\omega)| = \left|\frac{1}{-i\delta - \hbar\omega + \hbar\omega_{\mathbf{q}} - \frac{Ch}{s\hbar\omega + si\delta + h}}\right| , \tag{6.20}$$

where δ is a small imaginary part, which is added to $\hbar\omega$ to regularize the expression. Using eq. (6.20), using C from eq. (6.19) and tuning the resonance frequency to equal the spin splitting $\hbar\omega_0 = h$, gives the Greens functions for circularly polarized light shown in fig. 6.1. In fig. 6.1, the Greens function is multiplied by δ, to normalize the expression. The analytic solutions given by eq. (6.16) are also shown.

The resonance for the left-handed photons is not affected by the coupling to the ferromagnet and stays at ω_0. For right-handed photons, the interaction with the ferromagnetic metal induces an anti-crossing in the photon dispersion. The non-interacting resonance splits into two resonances symmetric about $\omega = \omega_0$. From eq. (2.26), one can see that a right-handed photon can flip the spin of an electron from up to down. Because of the spin splitting, flipping the spin absorbs the energy $\epsilon_{\mathbf{k},\downarrow} - \epsilon_{\mathbf{k},\uparrow} = h$. Since the cavity frequency is tuned to the spin splitting $\hbar\omega_0 = h$, this process is on-shell. On the other hand, the left-handed photons can flip the spin of an electron from down to up. This process frees the energy h and is therefore not on shell. Mathematically, this fact can be seen from the denominator in eq. (6.12) approaching zero for $s_{\mathrm{R}} = -1$.

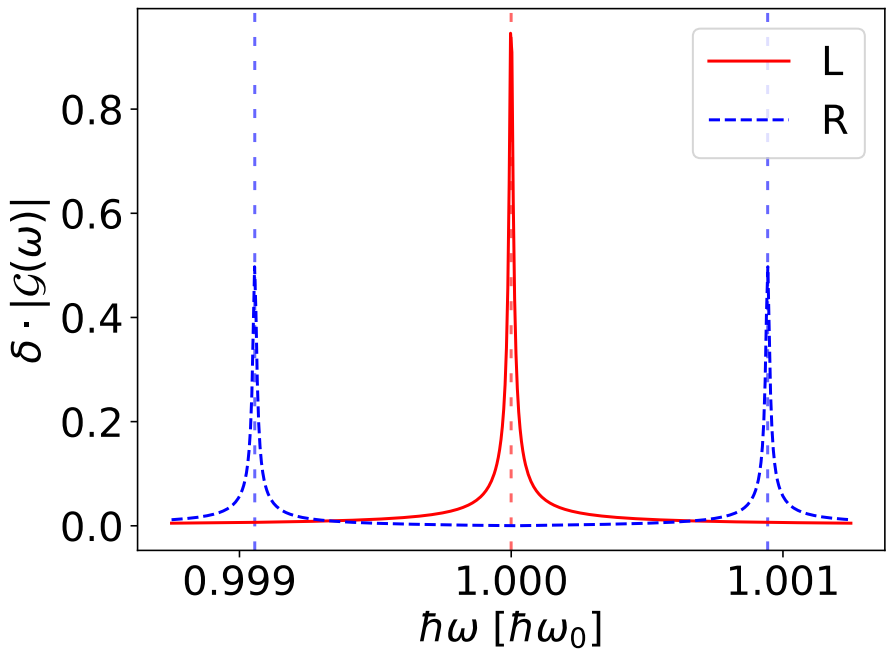

Figure 6.1: Resonances for left (L) and right (R) handed photons plotted against the frequency of the input signal. Resonances calculated using eq. (6.20), with $\delta = 5 \cdot 10^{-6}\hbar\omega_0$. Analytic solutions calculated with eq. (6.16) marked with horizontal lines.

In a transmission experiment, the resonance frequencies would be the same as in fig. 6.1. The amplitude would be given by eq. (3.16), and would be determined by the coupling of the cavity to the environment, the losses in the cavity, and the losses in the ferromagnet [22].

The splitting shown in fig. 6.1 could be observable in a real transmission experiment. For a spin splitting of $h = 1\,\text{meV}$ [42], the resonance condition $\hbar\omega_0 = h$, decides the energy scale $\omega_0/2\pi = h/(2\pi\hbar) = 243\,\text{GHz}$. With this energy scale, the splitting between the resonance frequencies equals $(\omega - \omega_0)/2\pi \approx 243\,\text{MHz}$. When considering the coupling between a ferrimagnet and an electromagnetic cavity, Huebl et al. resolved frequencies on the 10 MHz-scale [22]. Observing the anti-crossing would also require sufficiently small losses in the cavity and ferromagnetic metal. In the system studied by Huebl et al., the spin relaxation rate in the ferrimagnet was 50 MHz while the cavity relaxation rate was 3 MHz [22]. If our present system had similar loss rates, the losses would be sufficiently small to observe the anti-crossing. Meeting the resonance condition would require a cavity with a spacing in the z-direction given by $L_z = (\pi\hbar c)/h = 0.602\,\text{mm}$. These cavity dimensions are achievable [6]. The mode-splitting in our present setup could therefore be observable.

6.3 Ferromagnetic superconductor

The possibility of dichroism in a ferromagnetic metal leads naturally to the question of dichroism in a ferromagnetic superconductor. We model the ferromagnetic superconductor as a metal with spin-split bands where the up and down electrons have acquired gaps $\Delta_{\uparrow\uparrow}$ and $\Delta_{\downarrow\downarrow}$. In addition to the time-reversal symmetry breaking because of the spin-split bands, the gap parameters $\Delta_{\uparrow\uparrow}$ and $\Delta_{\downarrow\downarrow}$ can also spontaneously break time-reversal symmetry [12]. Such gap parameters will be considered in sections 6.4 to 6.6. In this section, the gap functions will be taken to be constant to simplify the numeric calculation of the resonances.

Placing the ferromagnetic superconductor at the bottom of the cavity and using the Zeeman interaction eq. (2.26) gives the action of the superconductor/electromagnetic cavity system

$$S = \sum_{ql} \left(-i\Omega_n + \omega_{\mathbf{q}}\right) a^\dagger_{al} a_{ql} + \sum_{kk'} \Psi^\dagger_k [\mathcal{G}^{-1}]_{kk'} \Psi_{k'} \ , \tag{6.21}$$

where $[\mathcal{G}^{-1}]_{kk'} = [\mathcal{G}_0^{-1}]_{kk'} + \chi_{kk'}$,

$$\mathcal{G}_0^{-1} = \begin{bmatrix} \epsilon_\uparrow(k) & 0 & \Delta_{\uparrow\uparrow}(k) & 0 \\ 0 & \epsilon_\downarrow(k) & 0 & \Delta_{\downarrow\downarrow}(k) \\ \bar{\Delta}_{\uparrow\uparrow}(k) & 0 & -\epsilon_\uparrow(-k) & 0 \\ 0 & \bar{\Delta}_{\downarrow\downarrow}(k) & 0 & -\epsilon_\downarrow(-k) \end{bmatrix} \delta_{k,k'} \ , \tag{6.22}$$

and

$$\chi_{kk'} = \tilde{g}_z \begin{bmatrix} 0 & -A_{k'-k\mathrm{L}} e^{-i\phi} & 0 & 0 \\ A_{k'-k\mathrm{R}} e^{i\phi} & 0 & 0 & 0 \\ 0 & 0 & 0 & A_{k'-k\mathrm{R}} e^{+i\phi} \\ 0 & 0 & -A_{k'-k\mathrm{L}} e^{-i\phi} & 0 \end{bmatrix} . \tag{6.23}$$

In the last line we defined $A_{k'-k\mathrm{R}} = \left(a_{k'-k\mathrm{R}} + a^\dagger_{k-k'\mathrm{L}}\right)$, $A_{k'-k\mathrm{L}} = \left(a_{k'-k\mathrm{L}} + a^\dagger_{k-k'\mathrm{R}}\right)$ and used the Nambu spinor eq. (5.4).

Performing the integral over the Nambu spinor and expanding the logarithm to second order, gives the effective photon action

$$S \approx \sum_{q,s} \left(-i\Omega_n + \omega_{\mathbf{q}}\right) a^\dagger_{a,s} a_{q,s} - \frac{1}{4} \mathrm{Tr}\Big\{ \left(\mathcal{G}_0 \chi\right)^2 \Big\} \ , \tag{6.24}$$

where there is an extra factor $\frac{1}{2}$ in front of the trace because the nambu spinor double counts the electron degrees of freedom [43, 44].

Computing the trace using Mathematica [45], and organizing the terms like eq. (6.2), gives us the expression for the coefficient

$$C_q^{\mathrm{LR}} = -\frac{\tilde{g}_z^2}{4} \sum_{k'} \frac{4\left(\left(-i\Omega_n - i\omega_{n'} + \epsilon_{\downarrow,\mathbf{k'}+\mathbf{q}}\right)\left(-i\omega_{n'} + \epsilon_{\uparrow,\mathbf{k'}}\right)\right)}{\left(E_\downarrow(\mathbf{k'}+\mathbf{q})^2 - \left(i\left(\Omega_n + \omega_{n'}\right)\right)^2\right)\left(E_\uparrow(\mathbf{k'}) - \left(i\omega_{n'}\right)^2\right)} \ . \tag{6.25}$$

In the last line we defined the quasiparticle energies $E_\uparrow = \sqrt{|\Delta_{\uparrow\uparrow}|^2 + \epsilon_{k,\uparrow}^2}$ and $E_\downarrow = \sqrt{|\Delta_{\downarrow\downarrow}|^2 + \epsilon_{k,\downarrow}^2}$. Taking the dipole approximation $\mathbf{q} = \mathbf{k} - \mathbf{k}' = 0$ and performing the matsubara summation over ω_n' gives

$$\begin{aligned} C_{i\Omega_n}^{\mathrm{LR}} = &-\frac{\tilde{g}_z^2}{4}\sum_{\mathbf{k}}\Big[\\ &\frac{2\left(E_\downarrow(\mathbf{k})-\epsilon_{\downarrow,\mathbf{k}}\right)\left(-i\Omega_n+E_\downarrow(\mathbf{k})-\epsilon_{\uparrow,\mathbf{k}}\right)n_F\left(E_\downarrow(\mathbf{k})\right)}{E_\downarrow(\mathbf{k})\left(-i\Omega_n+E_\downarrow(\mathbf{k})-E_\uparrow(\mathbf{k})\right)\left(-i\Omega_n+E_\downarrow(\mathbf{k})+E_\uparrow(\mathbf{k})\right)} \\ &-\frac{2\left(-E_\downarrow(\mathbf{k})-\epsilon_{\downarrow,\mathbf{k}}\right)\left(-i\Omega_n-E_\downarrow(\mathbf{k})-\epsilon_{\uparrow,\mathbf{k}}\right)n_F\left(-E_\downarrow(\mathbf{k})\right)}{E_\downarrow(\mathbf{k})\left(-i\Omega_n-E_\downarrow(\mathbf{k})-E_\uparrow(\mathbf{k})\right)\left(-i\Omega_n-E_\downarrow(\mathbf{k})+E_\uparrow(\mathbf{k})\right)} \\ &+\frac{2\left(i\Omega_n+E_\uparrow(\mathbf{k})-\epsilon_{\downarrow,\mathbf{k}}\right)\left(E_\uparrow(\mathbf{k})-\epsilon_{\uparrow,\mathbf{k}}\right)n_F\left(E_\uparrow(\mathbf{k})\right)}{E_\uparrow(\mathbf{k})\left(i\Omega_n+E_\uparrow(\mathbf{k})-E_\downarrow(\mathbf{k})\right)\left(i\Omega_m+E_\uparrow(\mathbf{k})+E_\downarrow(\mathbf{k})\right)} \\ &-\frac{2\left(i\Omega_n-E_\uparrow(\mathbf{k})-\epsilon_{\downarrow,\mathbf{k}}\right)\left(-E_\uparrow(\mathbf{k})-\epsilon_{\uparrow,\mathbf{k}}\right)n_F\left(-E_\uparrow(\mathbf{k})\right)}{E_\uparrow(\mathbf{k})\left(i\Omega_m-E_\uparrow(\mathbf{k})-E_\downarrow(\mathbf{k})\right)\left(i\Omega_m-E_\uparrow(\mathbf{k})+E_\downarrow(\mathbf{k})\right)}\Big] . \end{aligned} \tag{6.26}$$

We now make the simplifying assumption that $\Delta_{\uparrow\uparrow}$ and $\Delta_{\downarrow\downarrow}$ are constants. Assuming constant gap functions allows us to convert the sum over $\mathbf{k}$ to an integral over $\epsilon_\downarrow$

$$\begin{aligned} C_{i\Omega_n}^{\mathrm{LR}} = &-\frac{1}{4}\tilde{g}_z^2 C_k\int d\epsilon_\downarrow\Big[\\ &\frac{2\left(E_\downarrow(\epsilon_\downarrow)-\epsilon_\downarrow\right)\left(i\Omega_n+E_\downarrow(\epsilon_\downarrow)-\epsilon_\downarrow+h\right)n_F\left(E_\downarrow(\epsilon_\downarrow)\right)}{E_\downarrow(\epsilon_\downarrow)\left(-i\Omega_n+E_\downarrow(\epsilon_\downarrow)-E_\uparrow(\epsilon_\downarrow)\right)\left(-i\Omega_n+E_\downarrow(\epsilon_\downarrow)+E_\uparrow(\epsilon_\downarrow)\right)} \\ &-\frac{2\left(-E_\downarrow(\epsilon_\downarrow)-\epsilon_\downarrow\right)\left(-i\Omega_n-E_\downarrow(\epsilon_\downarrow)-\epsilon_\downarrow+h\right)n_F\left(-E_\downarrow(\epsilon_\downarrow)\right)}{E_\downarrow(\epsilon_\downarrow)\left(-i\Omega_n-E_\downarrow(\epsilon_\downarrow)-E_\uparrow(\epsilon_\downarrow)\right)\left(-i\Omega_n-E_\downarrow(\epsilon_\downarrow)+E_\uparrow(\epsilon_\downarrow)\right)} \\ &+\frac{2\left(i\Omega_n+E_\uparrow(\epsilon_\downarrow)-\epsilon_\downarrow\right)\left(E_\uparrow(\epsilon_\downarrow)-\epsilon_\downarrow+h\right)n_F\left(E_\uparrow(\epsilon_\downarrow)\right)}{E_\uparrow(\epsilon_\downarrow)\left(i\Omega_n+E_\uparrow(\epsilon_\downarrow)-E_\downarrow(\epsilon_\downarrow)\right)\left(i\Omega_m+E_\uparrow(\epsilon_\downarrow)+E_\downarrow(\epsilon_\downarrow)\right)} \\ &-\frac{2\left(i\Omega_n-E_\uparrow(\epsilon_\downarrow)-\epsilon_\downarrow\right)\left(-E_\uparrow(\epsilon_\downarrow)-\epsilon_\downarrow+h\right)n_F\left(-E_\uparrow(\epsilon_\downarrow)\right)}{E_\uparrow(\epsilon_\downarrow)\left(i\Omega_m-E_\uparrow(\epsilon_\downarrow)-E_\downarrow(\epsilon_\downarrow)\right)\left(i\Omega_m-E_\uparrow(\epsilon_\downarrow)+E_\downarrow(\epsilon_\downarrow)\right)}\Big] . \end{aligned} \tag{6.27}$$

Using eq. (6.4) the effective action for a single circular polarization is given by

$$S_{\mathrm{eff}}^l = \left(-i\hbar\Omega_n + \hbar\omega_0 - \frac{1}{4}\tilde{g}_z^2 C_k\int d\epsilon_\downarrow[...]_{i\Omega_n\to s_l i\Omega_n}\right)a_{q,i}^\dagger a_{q,i} . \tag{6.28}$$

Using eq. (4.17), the renormalized dispersion of the cavity is determined by the solutions of the equation

$$-\hbar\omega + \hbar\omega_0 - \frac{1}{4}\tilde{g}_z^2 C_k\int d\epsilon_\downarrow[...]_{i\Omega_n\to s_l(\omega+i\delta/\hbar)} = 0 , \tag{6.29}$$

where we have made the substitution $i\Omega_n \to \omega + i\delta/\hbar$ inside the integral. This equation is to complicated to be solved analytically, but the solutions can be found numerically by plotting the Greens function

$$\mathcal{G}(\omega) = \frac{1}{-\hbar\omega - i\delta + \hbar\omega_0 - \frac{1}{4}\tilde{g}_z^2 C_k\int d\epsilon_\downarrow[...]_{i\Omega_n\to s_l(\omega+i\delta/\hbar)}} , \tag{6.30}$$

where the solutions of eq. (6.29) will appear as sharp peaks in the frequency plot.

The Greens function for the ferromagnetic Superconductor calculated with eq. (6.30) is shown in fig. 6.2. In order to verify the numeric calculation, fig. 6.2a shows a plot of eq. (6.30) for $\Delta_{\uparrow\uparrow} = \Delta_{\downarrow\downarrow} = 0$. As expected, the Greens function spectrum is identical to the ferromagnet shown in fig. 6.1. Greens function for non-zero gaps are shown in figs. 6.2b to 6.2d. In fig. 6.2b, both the gap parameters are set to $0.05\hbar\omega_0$. In fig. 6.2c, $\Delta_{\uparrow\uparrow} = 0.05\hbar\omega_0$ and $\Delta_{\downarrow\downarrow} = 0$ while fig. 6.2d shows the plot for $\Delta_{\uparrow\uparrow} = 0$ and $\Delta_{\downarrow\downarrow} = 0.05\hbar\omega_0$.

When the electrons acquire a gap, the resonances for the left-handed photons remain virtually unchanged. For the right-handed photons, the resonance peak which resides above the bare photon resonance frequency $\hbar\omega_0$ vanishes and the resonance peak below the bare photon resonance moves closer to the bare resonance. This effect is related to the fact that the difference between the gapped quasiparticle spectra stops being in resonance with the photons $E_\downarrow - E_\uparrow \neq h = \hbar\omega_0$. The effect of the ferromagnetic metal on the photon dispersion, therefore stops being a simple anti-crossing.

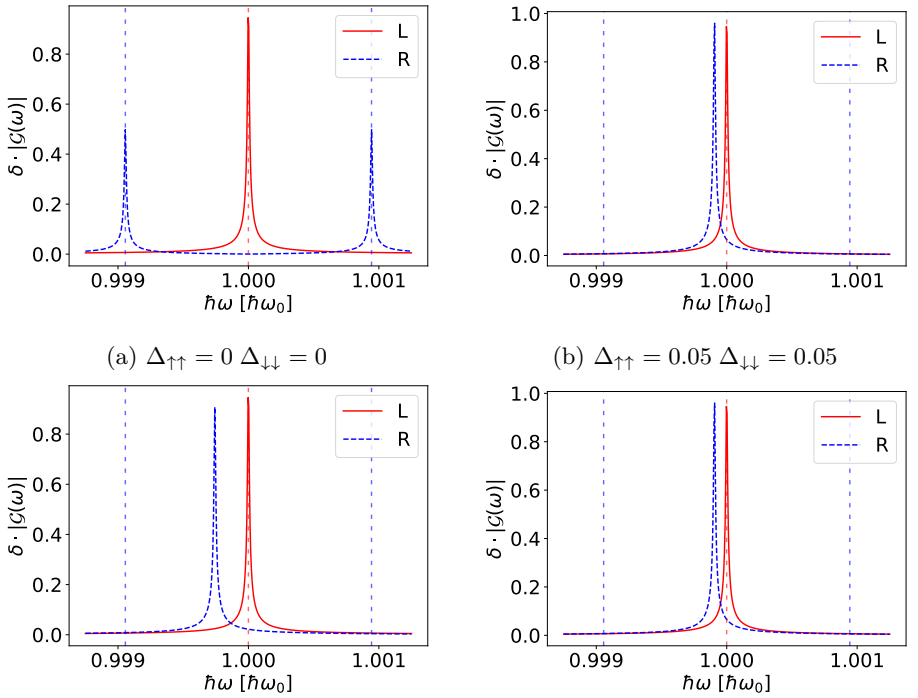

(a) $\Delta_{\uparrow\uparrow} = 0$ $\Delta_{\downarrow\downarrow} = 0$

(b) $\Delta_{\uparrow\uparrow} = 0.05$ $\Delta_{\downarrow\downarrow} = 0.05$

(c) $\Delta_{\uparrow\uparrow} = 0$ $\Delta_{\downarrow\downarrow} = 0.05$

(d) $\Delta_{\uparrow\uparrow} = 0.05$ $\Delta_{\downarrow\downarrow} = 0$

Figure 6.2: Green's functions for left and right-handed photons plotted against the frequency of the input signal. Calculated with eq. (6.29). Horizontal lines show analytic solutions for $\Delta_{\uparrow\uparrow} = \Delta_{\downarrow\downarrow} = 0$ calculated with eq. (6.16). Gap parameters given in units of $\hbar\omega_0$ and $\delta = 5 \cdot 10^{-6}\hbar\omega_0$.

6.4 One superconducting band

Time-reversal symmetry can also be broken by the superconducting gap. The simplest way to break the symmetry in this way would be if superconductivity only occurred in one of the spin bands. One possible gap symmetry where only spin-up electrons are superconducting is given by eq. (5.8). Taking only the $C_{k,\uparrow}$ electrons to be superconducting and integrating out all the electrons gives the effective photon theory

$$S[C^\dagger, C, a, a^\dagger] \approx \sum_{q,s} \left(-i\hbar\Omega_n + \hbar\omega_{\mathbf{q}}\right) a^\dagger_{q,s} a_{q,s} - \frac{1}{2}\,\mathrm{Tr}\left\{\left(\hat{\mathcal{G}}\hat{\chi}\right)^2\right\}, \tag{6.31}$$

where $\hat{\mathcal{G}}^{-1} = \hat{\mathcal{G}}_0^{-1} + \hat{\chi}$, with

$$\left[\mathcal{G}_0^{-1}\right]_{kk'} = \begin{bmatrix} \epsilon_k & 0 & \Delta^0_{\uparrow\uparrow}(k) & 0 \\ 0 & \epsilon_k & 0 & 0 \\ \bar{\Delta}^0_{\uparrow\uparrow}(k) & 0 & -\epsilon_{-k} & 0 \\ 0 & 0 & 0 & -\epsilon_{-k} \end{bmatrix} \delta_{kk'} \tag{6.32}$$

and where $\hat{\chi}$ is the same matrix as for the ferromagnetic superconductor, given by eq. (6.23). Computing the trace in eq. (6.31) using Mathematica [45] gives the coefficient

$$C_q^{\mathrm{LR}} = 2\sum_{k'} \frac{1}{\Delta^{k'}_{uu}\bar{\Delta}^{k'}_{uu} + \epsilon_{-k'}\epsilon_{k'}} \left(\frac{\epsilon_{k'}}{\epsilon_{-k'-q}} + \frac{\epsilon_{-k'}}{\epsilon_{k'+q}}\right). \tag{6.33}$$

This coefficient is invariant under the reversal of q, since reversing q and changing the order of summation $k' \to -k'$ leaves the expression invariant. Having superconductivity in only one of the spin bands is therefore not sufficient to get circular dichroism.

6.5 Non-unitary with two superconducting bands

We continue by analyzing the gap parameter given by eq. (5.9). This gap parameter is non-unitary but has superconductivity in both spin bands. In terms of the Nambu spinor eq. (5.4), the action of this superconductor is given by

$$\left[\mathcal{G}_0^{-1}\right]_{kk'} = \begin{bmatrix} \epsilon_k & 0 & -\Delta^0(k_x + k_y) & 0 \\ 0 & \epsilon_k & 0 & \Delta^0(k_x - k_y) \\ -\bar{\Delta}^0(k_x + k_y) & 0 & -\epsilon_{-k} & 0 \\ 0 & \bar{\Delta}^0(k_x - k_y) & 0 & -\epsilon_{-k} \end{bmatrix} \delta_{kk'} \tag{6.34}$$

Calculating $\mathrm{Tr}\left\{\left([\mathcal{G}_0^{-1}\hat{\chi}\right)^2\right\}$ for the Zeeman coupling at the bottom of the cavity (2.25) with mathematica [45], gives the expression for the coeficient

$$C_q^{\mathrm{LR}} = \sum_{k'} \frac{4\epsilon_{k'+q}\epsilon_{k'}}{E_{qk'}}. \tag{6.35}$$

In the last line, we defined

$$E_{qk'} = \frac{1}{\left(\left(k'_x + k'_y + q_x + q_y\right)^2 |\Delta|_0^2 + \epsilon_{k'+q}\epsilon_{-(k'+q)}\right)\left(\left(k'_x - k'_y\right)^2 |\Delta|_0^2 + \epsilon_{k'}\epsilon_{-k'}\right)} . \tag{6.36}$$

The coefficient in eq. (6.35) is not invariant when reversing the photon momentum and frequency, $C_q^{\mathrm{LR}} \neq C_{-q}^{\mathrm{LR}}$. The $\hat{x}k_x + i\hat{y}k_y$ gap symmetry could therefore give rise to circular dichroism.

In the dipole approximation $\mathbf{q} = \mathbf{k} - \mathbf{k}' = 0$, the coefficient becomes inn variant, $C_{i\Omega_n}^{\mathrm{LR}} = C_{-i\Omega_n}^{\mathrm{LR}}$. This can be verified by performing a $\pi/2$ rotation of $\mathbf{k}'$ and shifting the frequency $i\omega_{n'}$ by $i\Omega_n$ in the sum over k'. The combination of the small coupling constant for the Zeeman interaction discussed in section 6.2, and the effect vanishing in the dipole approximation means that the $\hat{x}k_x + i\hat{y}k_y$ gap symmetry would most likely give rise to a small dichroic signal.

6.6 Chiral superconductor

The chiral states with **d**-vectors $\hat{z}\left(k_x \pm ik_y\right)$ given in eq. (5.10) break time-reversal symmetry in the orbital part of the wave function [12]. The paramagnetic coupling describes the interaction between the electric field and the motion of the electrons in the crystal, making it the natural coupling to probe this chiral state. Using the paramagnetic coupling given in eq. (2.27) and integrating out the electron fields, gives the effective photon action

$$S[a, a^\dagger] \approx \sum_{q,l} \left(-i\hbar\Omega_n + \hbar\omega_{\mathbf{q}}\right) a_{ql}^\dagger a_{ql} - \frac{1}{2}\,\mathrm{Tr}\left\{\left(\sum_l \hat{\mathcal{G}}_0 \hat{\chi}_l\right)^2\right\}, \tag{6.37}$$

Where we have defined $\hat{\mathcal{G}}^{-1} = \hat{\mathcal{G}}_0^{-1} + \sum_s \hat{\chi}^s$,

$$\left[\hat{\mathcal{G}}_0^{-1}\right]_{kk'} = \begin{bmatrix} \epsilon_k & 0 & 0 & \Delta_0\left(k_x + ik_y\right) \\ 0 & \epsilon_k & \Delta_0\left(k_x + ik_y\right) & 0 \\ 0 & \bar{\Delta}_0\left(k_x - ik_y\right) & -\epsilon_{-k} & 0 \\ \bar{\Delta}_0\left(k_x - ik_y\right) & 0 & 0 & -\epsilon_{-k} \end{bmatrix} \delta_{kk'} , \tag{6.38}$$

and

$$\left[\hat{\chi}^l\right]_{kk'} = \frac{g^l_{\mathbf{k},\mathbf{k}'} A_{k-k',l}}{\sqrt{\beta}} \begin{bmatrix} 1 & 0 & 0 & 0 \\ 0 & 1 & 0 & 0 \\ 0 & 0 & 1 & 0 \\ 0 & 0 & 0 & 1 \end{bmatrix} . \tag{6.39}$$

In the last line, we picked the state $\hat{z}\left(k_x + ik_y\right)$ for convenience. When deriving the matrix $\hat{\chi}^s$ we used the identity $g^s_{-\mathbf{k}',-\mathbf{k}} = -g^s_{\mathbf{k},\mathbf{k}'}$. The trace in eq. (6.37)

becomes

$$\begin{aligned}\mathrm{Tr}\Big\{\Big(\hat{\mathcal{G}}_0\hat{\chi}\Big)^2\Big\} &= \sum_{k,k',s,s'} \mathrm{Tr}\Big\{\Big[\hat{\mathcal{G}}_0^{-1}\Big]_k [\hat{\chi}^s]_{kk'} \Big[\hat{\mathcal{G}}_0^{-1}\Big]_{k'} \Big[\hat{\chi}^{s'}\Big]_{k'k}\Big\} \\ &= \sum_{k,k',s,s'} \frac{g^s_{\mathbf{k},\mathbf{k}'}A_{k-k',s}}{\sqrt{\beta}} \frac{g^{s'}_{\mathbf{k}',\mathbf{k}}A_{k'-k,s'}}{\sqrt{\beta}} \mathrm{Tr}\Big\{\Big[\hat{\mathcal{G}}_0\Big]_k \Big[\hat{\mathcal{G}}_0\Big]_{k'}\Big\}\,,\end{aligned} \tag{6.40}$$

giving the coeficient

$$C_q^{\mathrm{LR}} = \frac{1}{\beta}\sum_{k'} \Big(g^{\mathrm{R}}_{(\mathbf{k}'+\mathbf{q})\mathbf{k}'}g^{\mathrm{L}}_{\mathbf{k}'(\mathbf{k}'+\mathbf{q})} + g^{\mathrm{L}}_{(\mathbf{k}'+\mathbf{q})\mathbf{k}'}g^{\mathrm{R}}_{\mathbf{k}'(\mathbf{k}'+\mathbf{q})}\Big) \mathrm{Tr}\Big\{\Big[\hat{\mathcal{G}}_0\Big]_{k'+q}\Big[\hat{\mathcal{G}}_0\Big]_{k'}\Big\}\,. \tag{6.41}$$

This coefficient is symmetric when reversing q. This can be seen by reversing q, shifting the summation variable $k' \to k'+q$, and using the trace identity $\mathrm{Tr}\{AB\} = \mathrm{Tr}\{BA\}$. Therefore, this system does not give rise to circular dichroism.

The inversion symmetry of eq. (6.41), does not depend on the explicit form of $\hat{\mathcal{G}}_0^{-1}$ given in eq. (6.38). The result is therefore not specific to chiral superconductors but holds for all electronic systems, coupled by the paramagnetic coupling in the center of the cavity. The paramagnetic coupling can therefore not give rise to dichroism in an input-output experiment. This is in contrast to dichroism in differential absorption experiments, where the paramagnetic coupling gives dichroism for several systems [30, 31]. For example, a metal with spin-orbit coupling in an external magnetic field would give rise to dichroism [30, 31].

The result in eq. (6.41) relies on using the identity $g^s_{-\mathbf{k}',-\mathbf{k}} = -g^s_{\mathbf{k},\mathbf{k}'}$ in the paramagnetic coupling coeficient eq. (2.27). As shown in section 2.5, this identity holds when modeling the metallic state as a free electron gas. Similarly, it holds when using a tight binding model on a square lattice [1, 25]. For a tight binding model on a lattice without inversion symmetry, this identity would not hold. Coupling the cavity and a material with such a lattice through the paramagnetic coupling could therefore give rise to circular dichroism. This is left as further work.

Chapter 7

Conclusion and outlook

In this thesis, we showed how one can extend the definition of circular dichroism from polarization-dependent absorption to polarization-dependent transmission in an electromagnetic cavity. In a transmission experiment, a condensed matter system is placed inside the electromagnetic cavity. Transmission experiments measure the renormalized dispersion of the cavity photons. The renormalized dispersion is calculated by constructing an effective theory for one polarization of light. Without the interaction with the condensed matter system, the left and right-handed photon dispersions are degenerate. In order to get circular dichroism in a transmission experiment, the effective photon theory resulting from the electron interactions must break this degeneracy. For interactions of the same form as the Zeeman and paramagnetic coupling, the left and right-handed photon bands split when the C_q^{LR}-part of the effective photon theory as defined by eq. (6.3) is not even under the reversal of $q = (-i\Omega_n, \mathbf{q})$.

As a first application of the procedure outlined above, we calculated the renormalized dispersion for a cavity interacting with a ferromagnetic metal placed at the bottom of the cavity. A ferromagnetic metal is a simple time-reversal symmetry-breaking system, which made it possible to calculate the renormalized dispersion analytically to second order. The calculation showed that a ferromagnetic metal would give rise to circular dichroism when interacting through the Zeeman coupling eq. (2.26). The renormalized photon spectrum for left-handed photons becomes unchanged. On the other hand, the renormalized photon spectrum for right-handed photons displays an anti-crossing with the ferromagnetic metal. The difference between left- and right-handed photons is caused by the right-handed photon processes being on-shell. For a two-dimensional ferromagnetic metal, this effect is too small to be detected. When considering a ferromagnetic metal of a finite thickness, the coupling increased by five orders of magnitude, making it feasible to detect the dichroism. The effect of the ferromagnetic metal can also be increased by tuning the resonance frequency of the cavity to equal the spin splitting in the ferromagnetic metal $\hbar\omega_{\mathbf{0}} = h$. These two techniques highlight the advantage of looking at light-matter coupling inside an electromagnetic cavity.

After studying the coupling between a cavity and a ferromagnetic metal, we

moved on to time-reversal symmetry-breaking superconductors. The first superconductor we considered was a ferromagnetic superconductor. The ferromagnetic superconductor is modeled as a metal with spin-split bands, with constant gaps $\Delta_{\uparrow\uparrow}$ and $\Delta_{\downarrow\downarrow}$. In contrast to the ferromagnetic metal, the difference between the quasiparticle energies can no longer be tuned to equal the spin splitting $E_\uparrow(k') - E_\downarrow(k') \neq h$. For this reason, the photon dispersion no longer displays an anti-crossing for the right-handed photons. Instead, the right-handed photons exhibit one resonance, which is below the non-interacting resonance. The left-handed photons are not affected by the interaction, in the same way as the ferromagnetic metal. As further work, one interesting possibility is to consider the effect of a ferromagnetic superconductor with a gap parameter that varies around the Fermi surface.

In the ferromagnetic superconductor, the time-reversal symmetry is broken in the ferromagnetic phase transition. Another possibility is for the time-reversal symmetry to be broken in the superconducting phase transition. In this case, the time-reversal symmetry is broken by the gap parameter $\Delta_{\sigma\sigma'}(\mathbf{k})$. A simple example of such a superconducting state is given by the **d**-vector $\mathbf{d}(\mathbf{k}) \propto (\hat{x} + i\hat{y})(k_x + ik_y)$. In this state, only the spin-up electrons are superconducting. However, this state does not give rise to dichroism in transmission experiments. Another state which breaks time-reversal symmetry is given by $\mathbf{d}(\mathbf{k}) = \hat{x}k_x + i\hat{y}k_y$. This state has gaps for both spin-up and spin-down electrons but with different variations around the Fermi surface. The effective photon theory for this state is not symmetric under the reversal of q, meaning that it could give rise to dichroism. However, the effect vanishes in the dipole approximation $\mathbf{q} = 0$. This has the consequence that the polarization dependency of the transmission experiment would be small.

In all the preceding cases, the time-reversal symmetry breaking occurred in the spin part of the state. In the ferromagnetic metal and ferromagnetic superconductor, the electron spins have a preferred direction. Similarly, the Cooper pairs in the states discussed in the previous paragraph also have a preferred spin direction. Therefore, the Zeeman coupling is the best choice to study these states, because it describes the interaction between the electron spins and the magnetic field. The chiral superconductor $\Delta(\mathbf{k}) \propto k_x \pm ik_y$, is an example of a state that breaks time-reversal symmetry in the orbital part of the wavefunction. The paramagnetic coupling describes the interaction between the electric field and the motion of the electrons in the material. This makes it a logical choice to study the chiral superconductor. However, the calculation showed that the paramagnetic coupling does not give rise to dichroism in a transmission experiment. Furthermore, the result was valid for all electronic states interacting with the electromagnetic cavity through the paramagnetic coupling. This points to a limitation of polarization-dependent transmission experiments because polarization-dependent absorption experiments can give rise to dichroism for certain states, like a metal with spin-orbit coupling wich is placed in a constant magnetic field. The result is dependent on having the symetry $g^s_{-\mathbf{k}',-\mathbf{k}} = -g^s_{\mathbf{k},\mathbf{k}'}$ in the paramagnetic coupling coeficient. This symmetry holds for a free electron gas and a tight-binding model on a square lattice. However, for tight binding models without inversion symmetry, the symmetry does not hold. Studying time-reversal

symmetry-breaking systems on these lattices is therefore an interesting possibility.

The main result of this thesis is the possibility of circular dichroism when an electromagnetic cavity is interacting with a ferromagnetic metal or superconductor. Since coupling electromagnetic cavities and condensed matter systems is a relatively new field of research, there are many possibilities to build on these results. In this thesis, we considered the paramagnetic- and Zeeman-coupling, which both couple the electromagnetic field to the quasiparticles in the superconductor. Another possibility is to couple the cavity to the Higgs mode, which is the field that describes the oscillations in the superconducting order parameter [1]. Moving away from superconductors, one possibility is to couple the cavity to a ferromagnetic insulator and to break the time-reversal symmetry with a spin-polarized spin current [46]. This time-reversal symmetry breaking could give rise to circular dichroism. Considering the spin current would require treating the system out of equilibrium.

Bibliography

[1] Eirik Jaccheri Høydalsvik. *Induced Superconductivity and Higgs Coupling in cavities (Project thesis)*. NTNU, 2022.

[2] Matthew D. Schwartz. *Quantum Field Theory and the Standard Model*. Cambridge University Press, 2014.

[3] S.W. Lovesey. *Topological Insulators and Topological Superconductors*. Princeton University Press, 2014.

[4] B. T. Thole et al. "X-ray circular dichroism as a probe of orbital magnetization". In: *Physical Review Letters* 68.12 (1992), pp. 1943–1946. DOI: 10.1103/PhysRevLett.68.1943.

[5] Tobias Funk et al. "X-ray magnetic circular dichroism - A high energy probe of magnetic properties". In: *Coordination Chemistry Reviews* 249.1-2 (2005), pp. 3–30. DOI: 10.1016/j.ccr.2004.05.017.

[6] F. Schlawin, D. M. Kennes, and M. A. Sentef. "Cavity quantum materials". In: *Applied Physics Reviews* 9.1 (2022). DOI: 10.1063/5.0083825.

[7] J. J. Henderson et al. "High-frequency microstrip cross resonators for circular polarization electron paramagnetic resonance spectroscopy". In: *Review of Scientific Instruments* 79.7 (2008), p. 074704. DOI: 10.1063/1.2957621.

[8] J. Diaz et al. "A microwave cavity for circularly polarized radiation". In: *Review of Scientific Instruments* 45.3 (1974), pp. 454–455. DOI: 10.1063/1.1686658.

[9] Sho Watanabe. *Circularly polarized microwaves for magnetic resonance experiments (Master thesis)*. Technische Universität München, 2015.

[10] Alexander Altland and Ben Simons. *Condensed Matter Field Theory*. Cambridge University Press, 2008.

[11] A P Mackenzie and Y Maeno. "p-wave superconductivity". In: *Physica B: Condensed Matter* 280 (2000), p. 148.

[12] Andrew Peter Mackenzie and Yoshiteru Maeno. "The superconductivity of Sr 2 RuO 4 and the physics of spin-triplet pairing". In: *Reviews of Modern Physics* 75 (2003).

[13] Andreas Halkjelsvik Mjøs. *Spontaneous Vortex Phase and Quantum Phase Diagram of Ferromagnetic Superconductors (Master thesis)*. NTNU, 2020.

[14] D. Fay and J. Appel. “Coexistence of p-state superconductivity and itinerant ferromagnetism”. In: *Physical Review B* 22.7 (1980), pp. 3173–3182. DOI: 10.1103/PhysRevB.22.3173.

[15] E. K. Dahl and A. Sudbø. “Derivation of the Ginzburg-Landau equations for a ferromagnetic p -wave superconductor”. In: *Physical Review B* 75.14 (2007), p. 144504. DOI: 10.1103/PhysRevB.75.144504.

[16] Dai Aoki et al. “Coexistence of superconductivity and ferromagnetism in URhGe”. In: *Nature* 413.01 (2001), pp. 27–36.

[17] N. T. Huy et al. “Superconductivity on the border of weak itinerant ferromagnetism in UCoGe”. In: *Physical Review Letters* 99.6 (2007), p. 067006. DOI: 10.1103/PhysRevLett.99.067006.

[18] S S. Saxena et al. “Superconductivity on the border of itinerant-electron ferromagnetism in UGe 2”. In: *Nature* 406.August (2000), pp. 587–592.

[19] Catherine Kallin and John Berlinsky. “Chiral superconductors”. In: *Reports on Progress in Physics* 79.5 (2016), p. 054502. DOI: 10.1088/0034-4885/79/5/054502.

[20] K. Kakazu and Y. S. Kim. “Quantization of electromagnetic fields in cavities and spontaneous emission”. In: *Physical Review A* 50.2 (1994), pp. 1830–1839. DOI: 10.1103/PhysRevA.50.1830.

[21] Ö. O. Soykal and M E Flatté. “Strong Field Interactions between a Nanomagnet and a Photonic Cavity”. In: *Physical Review Letters* 104.7 (2010), p. 077202. DOI: 10.1103/PhysRevLett.104.077202.

[22] Hans Huebl et al. “High Cooperativity in Coupled Microwave Resonator Ferrimagnetic Insulator Hybrids”. In: *Physical Review Letters* 111.12 (2013), p. 127003. DOI: 10.1103/PhysRevLett.111.127003.

[23] Yutaka Tabuchi et al. “Hybridizing ferromagnetic magnons and microwave photons in the quantum limit”. In: *Physical Review Letters* 113.8 (2014), p. 083603. DOI: 10.1103/PhysRevLett.113.083603.

[24] Øyvind Johansen and Arne Brataas. “Nonlocal Coupling between Antiferromagnets and Ferromagnets in Cavities”. In: *Physical Review Letters* 121.8 (2018), p. 87204. DOI: 10.1103/PhysRevLett.121.087204.

[25] Frank Schlawin, Andrea Cavalleri, and Dieter Jaksch. “Cavity-Mediated Electron-Photon Superconductivity”. In: *Physical Review Letters* 122.13 (2019). DOI: 10.1103/PhysRevLett.122.133602.

[26] Andreas T.G. Janssønn et al. “Macroscale nonlocal transfer of superconducting signatures to a ferromagnet in a cavity”. In: *Physical Review B* 102.18 (2020), 180506(R). DOI: 10.1103/PhysRevB.102.180506.

[27] Andreas T.G. Janssønn. “Cavity-mediated impact of superconductors on ferromagnetic insulators”. PhD thesis. NTNU, 2022.

[28] Dany Lachance-Quirion et al. “Resolving quanta of collective spin excitations in a millimeter-sized ferromagnet”. In: *Science Advances* 3.7 (2017), e1603150. DOI: 10.1126/sciadv.1603150.

[29] Yutaka Tabuchi et al. “Coherent coupling between a ferromagnetic magnon and a superconducting qubit”. In: *Science* 349.6246 (2015), pp. 405–408. DOI: 10.1126/science.aaa3693.

[30] K. Capelle, E. K.U. Gross, and B. L. Györffy. “Theory of dichroism in the electromagnetic response of superconductors”. In: *Physical Review Letters* 78.19 (1997), pp. 3753–3756. DOI: 10.1103/PhysRevLett.78.3753.

[31] K. Capelle, E. Gross, and B. Györffy. “Analysis of dichroism in the electromagnetic response of superconductors”. In: *Physical Review B - Condensed Matter and Materials Physics* 58.1 (1998), pp. 473–489. DOI: 10.1103/PhysRevB.58.473.

[32] K. I. Wysokiński, James F. Annett, and B. L. Györffy. “Intrinsic optical dichroism in the chiral superconducting state of Sr 2RuO 4”. In: *Physical Review Letters* 108.7 (2012), p. 077004. DOI: 10.1103/PhysRevLett.108.077004.

[33] Karol I. Wysokiński, James F. Annett, and Balazs L. Györffy. “Intrinsic optical Dichroism in the 2D model of Chiral superconducting state”. In: *Journal of Superconductivity and Novel Magnetism* 26.5 (2013), pp. 1909–1913. DOI: 10.1007/s10948-012-2046-7.

[34] S. K. Yip and J. A. Sauls. “Circular dichroism and birefringence in unconventional superconductors”. In: *Journal of Low Temperature Physics* 86.3-4 (1992), pp. 257–290. DOI: 10.1007/BF01151804.

[35] Q. P. Li and Robert Joynt. “Theory of dichroism in high-temperature superconductors”. In: *Physical Review B* 44.9 (1991), pp. 4720–4723. DOI: 10.1103/PhysRevB.44.4720.

[36] Denis G. Baranov et al. “Circular dichroism mode splitting and bounds to its enhancement with cavity-plasmon-polaritons”. In: *Nanophotonics* 9.2 (2020), pp. 283–293. DOI: 10.1515/nanoph-2019-0372.

[37] Andreas T.G. Janssønn et al. “Cavity-mediated superconductor-ferromagnetic-insulator coupling”. In: *Physical Review B* 107.3 (2023), p. 035147. DOI: 10.1103/PhysRevB.107.035147.

[38] Jacob Linder. *Intermediate Quantum Mechanics*. Bookboon, 2018. DOI: 10.1201/9780429493645.

[39] D.F.Walls. *Quantom Optics*. Springer-Verlag Berlin Heidelberg, 1994.

[40] J. Linder and A. Sudbø. “Quantum transport in noncentrosymmetric superconductors and thermodynamics of ferromagnetic superconductors”. In: *Physical Review B* 76.5 (2007), p. 054511. DOI: 10.1103/PhysRevB.76.054511.

[41] A. Pustogow et al. “Constraints on the superconducting order parameter in Sr2RuO4 from oxygen-17 nuclear magnetic resonance”. In: *Nature* 574.7776 (2019), pp. 72–75. DOI: 10.1038/s41586-019-1596-2.

[42] Sol H. Jacobsen, Jabir Ali Ouassou, and Jacob Linder. "Critical temperature and tunneling spectroscopy of superconductor-ferromagnet hybrids with intrinsic Rashba-Dresselhaus spin-orbit coupling". In: *Physical Review B - Condensed Matter and Materials Physics* 92.2 (2015), p. 024510. DOI: 10.1103/PhysRevB.92.024510.

[43] Franz Wegner. *Supermathematics and its applications in statistical physics : Grassmann variables and the method of supersymmetry*. Springer-Verlag Berlin Heidelberg, 2016.

[44] Henning G. Hugdal et al. "Inverse proximity effect in s -wave and d -wave superconductors coupled to topological insulators". In: *Physical Review B* 99.9 (2019), p. 094505. DOI: 10.1103/PhysRevB.99.094505.

[45] Inc Wolfram Research. *Mathematica*. Champaign, Illinois, 2022.

[46] Ran Cheng et al. "Spin pumping and spin-transfer torques in antiferromagnets". In: *Physical Review Letters* 113.5 (2014), p. 057601. DOI: 10.1103/PhysRevLett.113.057601.

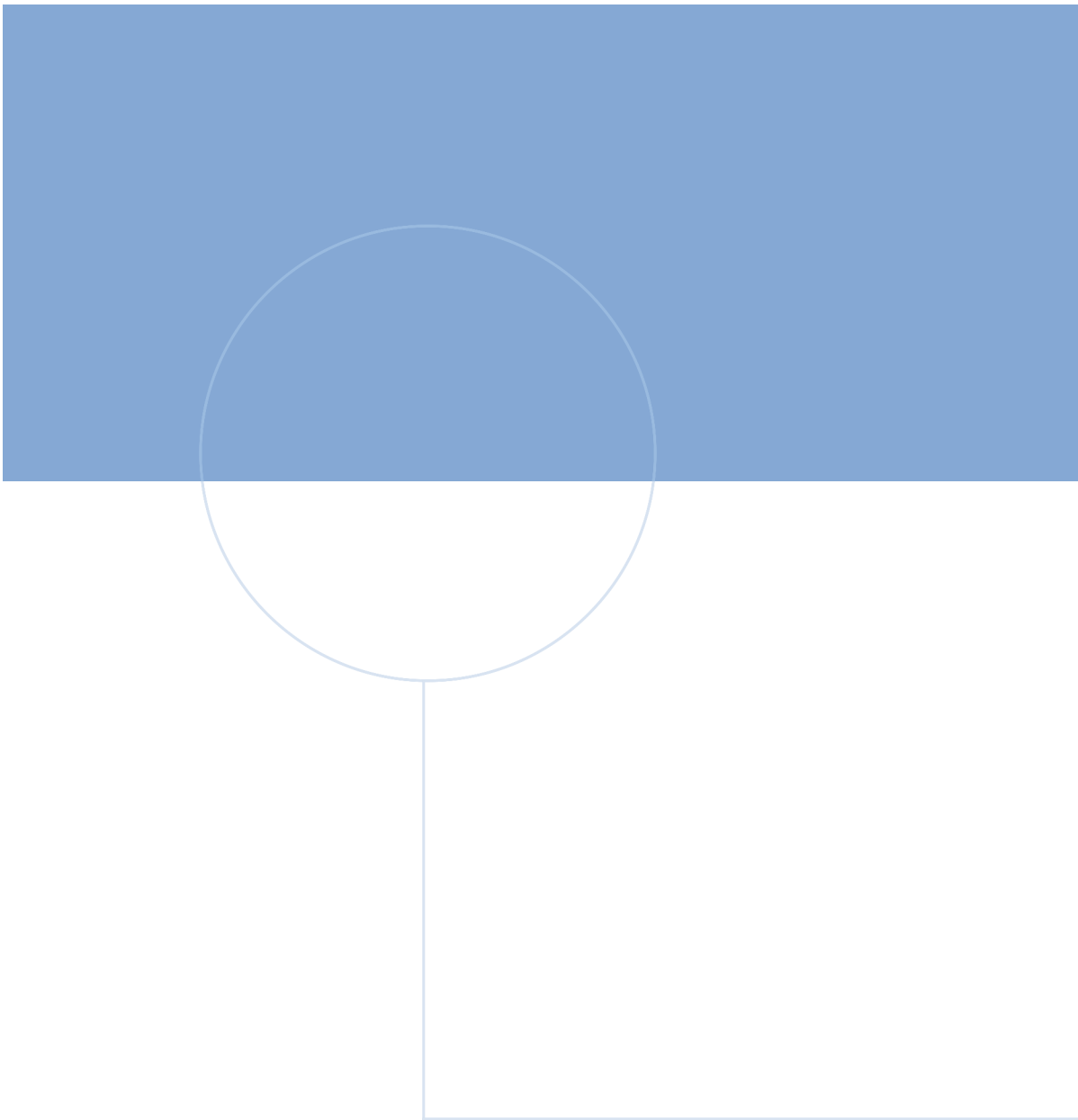

NTNU

Norwegian University of
Science and Technology